Theses and Dissertations   1. Thesis and Dissertation Collection, all items

1996-06

Range-dependent passive source localization using data from the Barents Sea tomography experiment

Pierce, David D.

Monterey, California. Naval Postgraduate School

https://hdl.handle.net/10945/8881

NAVAL POSTGRADUATE SCHOOL
MONTEREY, CALIFORNIA

DISSERTATION

RANGE-DEPENDENT PASSIVE SOURCE
LOCALIZATION USING DATA FROM THE
BARENTS SEA TOMOGRAPHY EXPERIMENT

by

David D. Pierce

June, 1996

Dissertation Supervisors: Charles Therrien
Ching-Sang Chiu
James Miller

Approved for public release; distribution is unlimited.

REPORT DOCUMENTATION PAGE		Form Approved OMB No. 0704-0188

Public reporting burden for this collection of information is estimated to average 1 hour per response, including the time for reviewing instruction, searching existing data sources, gathering and maintaining the data needed, and completing and reviewing the collection of information. Send comments regarding this burden estimate or any other aspect of this collection of information, including suggestions for reducing this burden, to Washington Headquarters Services, Directorate for Information Operations and Reports, 1215 Jefferson Davis Highway, Suite 1204, Arlington, VA 22202-4302, and to the Office of Management and Budget, Paperwork Reduction Project (0704-0188) Washington DC 20503

1. AGENCY USE ONLY (Leave blank)	2. REPORT DATE June 1996.	3. REPORT TYPE AND DATES COVERED Doctoral Dissertation

4. TITLE AND SUBTITLE RANGE-DEPENDENT PASSIVE SOURCE LOCALIZATION USING DATA FROM THE BARENTS SEA TOMOGRAPHY EXPERIMENT	5. FUNDING NUMBERS
6. AUTHOR(S) Pierce, David D.	
7. PERFORMING ORGANIZATION NAME(S) AND ADDRESS(ES) Naval Postgraduate School Monterey CA 93943-5000	8. PERFORMING ORGANIZATION REPORT NUMBER
9. SPONSORING/MONITORING AGENCY NAME(S) AND ADDRESS(ES)	10. SPONSORING/MONITORING AGENCY REPORT NUMBER

11. SUPPLEMENTARY NOTES The views expressed in this thesis are those of the author and do not reflect the official policy or position of the Department of Defense or the U.S. Government.

12a. DISTRIBUTION/AVAILABILITY STATEMENT Approved for public release; distribution is unlimited.	12b. DISTRIBUTION CODE

13. ABSTRACT (maximum 200 words)
Matched-Field Processing (MFP) and Matched-Mode Processing (MMP) are two popular techniques for passively localizing an underwater acoustic emitter in range and depth. One major drawback of these techniques has been their sensitivity to uncertainty concerning the acoustic environment. Several methods for addressing this phenomenon have been proposed in the literature, with varying degrees of success. Achieving high-quality location estimates remains a problem except in simple range-independent experiments or numerical simulations. In this study, we demonstrate an approach for robust, accurate emitter localization in a highly range-dependent real environment using MMP. The main factors contributing to successful localization are: 1) use of the high-resolution Multiple Signal Classification (MUSIC) algorithm, which performs well even when only a few robust modes can be obtained by mode filtering; and 2) use of an acoustic propagation model incorporating mode coupling, which is able to generate accurate replica fields in a strongly range-dependent environment. A secondary objective of the study was to demonstrate the application of higher-order statistical estimation techniques to reduce noise effects. Our results indicate that these techniques show unacceptable sensitivity to noise- and model-induced estimation errors and require further refinement before they will be useful in the underwater acoustic localization problem.

14. SUBJECT TERMS Matched-Field Processing, Source Localization	15. NUMBER OF PAGES 95
	16. PRICE CODE

17. SECURITY CLASSIFICATION OF REPORT Unclassified	18. SECURITY CLASSIFICATION OF THIS PAGE Unclassified	19. SECURITY CLASSIFICATION OF ABSTRACT Unclassified	20. LIMITATION OF ABSTRACT UL

RANGE-DEPENDENT PASSIVE SOURCE LOCALIZATION USING DATA FROM THE BARENTS SEA TOMOGRAPHY EXPERIMENT

David D. Pierce
Lieutenant Commander, United States Navy
B.S., University of Rochester, 1983
M.S., Naval Postgraduate School, 1989

DOCTOR OF PHILOSOPHY IN ENGINEERING ACOUSTICS

from the

NAVAL POSTGRADUATE SCHOOL
June 1996

ABSTRACT

Matched-Field Processing (MFP) and Matched-Mode Processing (MMP) are two popular techniques for passively localizing an underwater acoustic emitter in range and depth. One major drawback of these techniques has been their sensitivity to uncertainty concerning the acoustic environment. Several methods of addressing this phenomenon have been proposed in the literature, with varying degrees of success. Achieving high-quality location estimates remains a problem except in simple range-independent experiments or numerical simulations. In this study, we demonstrate an approach for robust, accurate emitter localization in a highly range-dependent real environment using MMP. The main factors contributing to successful localization are: 1) use of the high-resolution Multiple Signal Classification (MUSIC) algorithm, which performs well even when only a few robust modes can be obtained by mode filtering; and 2) use of an acoustic propagation model incorporating mode coupling, which is able to generate accurate replica fields in a strongly range-dependent environment. A secondary objective of the study was to demonstrate the application of higher-order statistical estimation techniques to reduce noise effects. Our results indicate that these techniques show unacceptable sensitivity to noise- and model-induced estimation errors and require further refinement before they will be useful in the underwater acoustic localization problem.

TABLE OF CONTENTS

ACKNOWLEDGMENT

I. INTRODUCTION

Throughout the history of anti-submarine warfare, there has been great interest in the use of passive acoustic measurements to localize submarines. Numerous methods of estimating the Direction-Of-Arrival (DOA) of acoustic emissions from a target of interest have been developed over the years for sonar applications. However, these techniques are inherently incapable of directly determining the range and depth of a target (emitter), although there are indirect means of determining range by observing target DOA as a function of time. Because knowledge of range and depth is so vital in military applications, there has been considerable interest in developing techniques for direct determination of these parameters. One such technique, which has attracted considerable attention in recent years, is a generalization of DOA estimation known as Matched-Field Processing (MFP), along with a variation on MFP known as Matched-Mode Processing (MMP).

Because of the similarity between DOA estimation and MFP/MMP, many of the techniques used in DOA estimation may be generalized for use in MFP/MMP. Two of the most popular DOA estimation methods—Bartlett and Minimum-Variance—have been studied extensively in the context of MFP (although the Minimum-Variance method has not been addressed in MMP) [Refs. 1, 2, 3, 4, 5, 6]. The MUSIC method has received extensive coverage in the DOA estimation literature, but relatively scant attention in the MFP literature [Refs. 7, 8, 9] and no attention in the MMP literature, possibly because of a perception that it would not perform well in realistic underwater acoustic environments.

1

One of the most noteworthy results from MFP/MMP studies to date is the great sensitivity of the location estimates to uncertain knowledge of the acoustic environment. Numerous researchers [Refs. 10, 11, 12, 13, 14, 15] have studied this phenomenon and proposed various methods for addressing it, with varying degrees of success. The problem remains an open issue. Because of this sensitivity, and also because of the limited availability of real data sets, most MFP/MMP research to date has involved either simple range-independent experiments or numerical simulations.

The objectives of this dissertation are to:

- Demonstrate the application of MFP/MMP to experimental data obtained in a strongly range-dependent environment during the 1992 Barents Sea Polar Front Experiment [Refs. 16, 17, 18, 19];

- Demonstrate that a coupled-mode propagation model is able to model the acoustic fields used in MFP/MMP with sufficient accuracy for high-quality localization estimates;

- Demonstrate that the high resolution of the MUSIC algorithm in combination with MMP is able to produce accurate location estimates in a realistic environment; and

- Demonstrate the application of higher-order statistics to the MFP/MMP problem. Although such methods have received some attention in the DOA estimation literature [Refs. 20, 21, 22], they have not yet been applied to MFP/MMP.

Chapter II gives an overview of pertinent background material, including DOA estimation algorithms, modeling of underwater sound

propagation, and MFP/MMP theory. In that chapter, we: describe three of the most popular DOA estimation algorithms—the Bartlett, Minimum-Variance, and MUSIC methods; review the modeling of the acoustic field via decomposition into normal modes for both range-dependent and range-independent environments; discuss the application of higher-order statistics to DOA estimation; and derive the extension of DOA estimation techniques to MFP/MMP. Except for the portion regarding application of the MUSIC algorithm and higher-order statistics to MMP, this chapter contains no original material. Chapter III gives a brief overview of those features of the Barents Sea Polar Front Experiment which are relevant to this dissertation, including the physical characteristics of the channel and a description of the emitter and receiver. Chapter IV provides additional information concerning the data analysis procedure; it also presents and interprets the results of the analysis. Chapter V gives the conclusions reached from the research and proposes areas for further investigation.

II. BACKGROUND

This chapter provides the framework for our analytical approach. It includes overviews of the following topics: DOA estimation fundamentals, including an extensive description of the MUSIC algorithm; application of higher-order statistics to DOA estimation; normal mode modeling of the acoustic field; and theoretical foundations of MFP/MMP.

A. DOA ESTIMATION

One of the most fundamental parameters of interest in military applications is the Direction-of-Arrival (DOA) corresponding to a target of interest. This parameter is one of the primary outputs of virtually all military radar and sonar systems. DOA may be expressed in terms of azimuth (bearing) and/or elevation. Over the years, numerous techniques have been developed for DOA estimation (for a good overview, see [Ref. 23] and references therein); the most important of these techniques are discussed briefly in this chapter. As we will see later, these techniques may be generalized in a straightforward manner for use in Matched-Field Processing.

1. Signal Model

As is generally the case in signal processing algorithms, DOA estimation techniques make certain assumptions about the signals being processed. They assume, in particular, that the sound pressure field in the underwater acoustic channel may be expressed as a plane wave (*i.e.*, that the surfaces of constant phase are planar). As we will see later, this assumption is not true in general, but is useful in many cases of practical interest. We will also assume that the signal is temporally narrowband with center frequency ω; *i.e.,* that amplitude and phase modulation do not introduce

5

appreciable amplitude and phase changes over the physical extent (length) of the receiving array. If a signal does not satisfy this latter condition, the signal may be decomposed via Fourier techniques into narrowband components which do satisfy the condition. For the sake of generality, during most of the background discussions, we will allow the number of emitters to be arbitrary, even though the presence of a single emitter will be assumed during all actual data analysis.

For mathematical convenience, we will conduct our analysis using the complex envelope representation of the signal rather than the real (physical) signal itself. Thus, if $s(t)$ is the real signal, the corresponding *analytic signal* or *pre-envelope* [Ref. 24] is given by

$$\tilde{s}(t) = s(t) + j\hat{s}(t),$$

where $\hat{s}(t)$ is the Hilbert transform of $s(t)$,

$$\hat{s}(t) = \int_{-\infty}^{\infty} \frac{s(\varsigma)}{t-\varsigma} d\varsigma.$$

The pre-envelope of a real bandpass signal at center frequency ω may be determined as follows [Ref. 25]:

- Multiply the real signal $s(t)$ by the complex carrier $\exp(j\omega t)$;

- Pass the resulting signal through a low-pass filter to remove the component at twice the carrier frequency;

- Multiply the resulting baseband signal by the complex carrier.

All signals appearing in the sequel will be the pre-envelopes of real narrowband signals unless otherwise indicated. The narrowband assumption

6

mentioned earlier is equivalent to requiring the complex pre-envelope of the received signal to be of the form

$$s(t) = S_i \exp(j\omega t),$$

where the (complex) amplitude S_i is a slowly varying function of time, *i.e.,*

$$S_i(t) \approx S_i\left(t - \frac{l}{v}\right),$$

where l is the length of the array and v is the speed of sound.

The concept of an *array response vector* is one that arises often in DOA estimation and MFP. To illustrate this concept, we consider an arbitrary receiving array of N elements. We may represent the signal as an N-dimensional, time-varying, complex vector whose components are the signals at the individual array elements. For convenience, we will assume that only the azimuth θ of the target is of interest, although extension to include dependence on elevation is straightforward. In DOA estimation, the array response vector $\mathbf{a}(\theta)$ is defined to be the unit-normalized (*i.e.,* length of $\mathbf{a}(\theta)$=1), noise-free, pressure field vector expected (based on the modeling assumptions) at the receive array given that an emitter is at the angle θ. The set of $\mathbf{a}$ vectors for all possible values of θ is known as the *array manifold*. More generally, $\mathbf{a}$ could be a function of parameters other than DOA as well. For the simple case involving a single emitter, a receiving array of N identical, omnidirectional elements in an arbitrary geometry and a narrowband, plane-wave signal with center frequency ω, $\mathbf{a}(\theta)$ may be expressed as

$$\mathbf{a}(\theta) = \frac{1}{\sqrt{N}}\begin{bmatrix} 1 & e^{-j\omega\tau_1} & \cdots & e^{-j\omega\tau_{N-1}} \end{bmatrix}^T,$$

where τ_i (a function of θ) represents the time delay seen by the incoming plane wave between sensor i and sensor 0 and superscript T denotes (non-conjugate) matrix transpose. In the general case where d emitters are present, the signal model used in DOA estimation is

$$\mathbf{p} = \mathbf{As} + \mathbf{n}, \tag{1}$$

where $\mathbf{p} = \begin{bmatrix} p_1(t) & p_2(t) & \cdots & p_N(t) \end{bmatrix}^T$ and $\mathbf{n} = \begin{bmatrix} n_1(t) & n_2(t) & \cdots & n_N(t) \end{bmatrix}^T$ are vectors whose elements are the received pressure and noise, respectively, at each element of the array; $\mathbf{s} = \begin{bmatrix} s_1(t) & s_2(t) & \cdots & s_d(t) \end{bmatrix}^T$ is the vector of signals produced by the d emitters ($s_i(t)=S_i\exp(j\omega t)$, with S_i a complex amplitude, because of the narrowband assumption); $\mathbf{A} = \begin{bmatrix} \mathbf{a}(\theta_1) & \mathbf{a}(\theta_2) & \cdots & \mathbf{a}(\theta_d) \end{bmatrix}$ is a matrix whose columns are the array response vectors corresponding to the DOAs of the d emitters; and t is time. Assuming that the signal and noise are uncorrelated, the signal-plus-noise covariance matrix $\mathbf{R_p}$ is then given by

$$\begin{aligned} \mathbf{R_p} &= E\begin{bmatrix} \mathbf{pp}^H \end{bmatrix} \\ &= \mathbf{AR_s A}^H + \mathbf{R_n}, \end{aligned} \tag{2}$$

where $\mathbf{R_s} = E\begin{bmatrix} \mathbf{ss}^H \end{bmatrix}$ and $\mathbf{R_n} = E\begin{bmatrix} \mathbf{nn}^H \end{bmatrix}$ are the signal and noise covariance matrices, respectively, superscript H denotes Hermitian (conjugate) transpose and E denotes statistical expectation. An estimate of $\mathbf{R_p}$ derived from the measured data is the fundamental quantity used in virtually all DOA estimation algorithms studied to date.

2. Algorithms

Numerous signal processing algorithms have been studied in the context of DOA estimation. Many are fairly obvious generalizations of techniques used for estimating the spectra of time series.

a. Weighted-sum beamforming

Weighted-sum beamforming (see, for example, [Ref. 26]) is the most commonly used technique (in practice) for DOA estimation, and is used in virtually all modern military radar and sonar systems. This technique is analogous to the Finite Impulse Response (FIR) filters used in time-series analysis. The output $b(t)$ of the beamformer is simply a linear combination of the signals received by the elements of the array,

$$b(t) = \mathbf{w}^H \mathbf{p}(t),$$

where $\mathbf{w}$ is the vector of weights. The weight vector $\mathbf{w}$ is chosen to satisfy a statistical constraint which is appropriate for the given situation. The expected value B of the output power of the beamformer is given by

$$B = E\left[|b(t)|^2\right] = \mathbf{w}^H \mathbf{R_p} \mathbf{w}. \tag{3}$$

A particular value for $\mathbf{w}$ generally produces high gain only in a single look direction, *i.e.*, for a single value of θ. In practice, multiple look directions are of interest, so that multiple $\mathbf{w}$ vectors are required (this approach is analogous to the use of a "bank" of matched filters in, for example, active sonar). Thus, in general, both $\mathbf{w}$ and B are functions of θ. The value of θ for which B is maximized is taken as the estimated DOA of the emitter; this value may be obtained by conventional one-dimensional search techniques.

The Bartlett beamformer is a special case of weighted-sum beamforming in which the weight vectors $\mathbf{w}$ are simply the array response vectors $\mathbf{a}$ for all look directions of interest. When the noise is spatially homogeneous, it can be easily shown that the output of this beamformer has the highest possible Signal-to-Noise Ratio (SNR) of any weighted-sum beamformer. This beamformer is analogous to the periodogram [Ref. 27] used

in time-series analysis. Since for the Bartlett beamformer $\mathbf{w}=\mathbf{a}(\theta)$, the expected value of the output power of the beamformer is

$$B(\theta) = \mathbf{a}^H(\theta)\mathbf{R}_\mathbf{p}\mathbf{a}(\theta) \qquad (4)$$

and the DOA estimate is given by

$$\hat{\theta} = \arg\max \mathbf{a}^H(\theta)\mathbf{R}_\mathbf{p}\mathbf{a}(\theta).$$

The Minimum-Variance method (MVM), also (somewhat misleadingly) known as the "Maximum Likelihood" (ML) beamformer [Refs. 28, 29] selects the beamformer weights to minimize the beamformer output power, subject to the constraint of unity gain (*i.e.*, zero distortion) in the desired look direction θ. Formally, $\mathbf{w}$ is chosen to

$$\text{minimize } \mathbf{w}^H\mathbf{R}_\mathbf{p}\mathbf{w}$$
$$\text{subject to } \mathbf{w}^H\mathbf{a}(\theta) = 1.$$

The effect of this minimization is to produce the lowest array response at directions that have the strongest signals. Thus, this method is useful in reducing the effects of directional noise on beamformer performance. The required weights may be easily shown (*e.g.*, [Ref. 23]) (using the method of Lagrange multipliers) to be

$$\mathbf{w}(\theta) = \frac{\mathbf{R}_\mathbf{p}^{-1}\mathbf{a}(\theta)}{\mathbf{a}^H(\theta)\mathbf{R}_\mathbf{p}^{-1}\mathbf{a}(\theta)}.$$

Substituting into (3) and simplifying gives a beamformer output power of

$$B(\theta) = \frac{1}{\mathbf{a}^H(\theta)\mathbf{R}_\mathbf{p}^{-1}\mathbf{a}(\theta)}. \qquad (5)$$

For a comparison of the performance of the Bartlett and MVM techniques, see Lacoss [Ref. 29].

b.   MUSIC

The MUSIC (for MUltiple SIgnal Classification) method [Refs. 30, 31, 32] is one of the first and probably the most widely studied of a class of techniques which address the DOA estimation problem from a geometric perspective; such methods offer potentially large improvements in resolution with respect to beamforming [Ref. 23]. Because MUSIC is central to the investigations of this dissertation, a full discussion of it is provided in the sequel. This discussion will attempt to develop an intuitive understanding of the algorithm rather than to provide a rigorous proof of its methods.

Signal Subspace. Figure 1 is a geometric illustration of the behavior of the received signal vector $\mathbf{p}(t)$ due to d emitters at various DOAs. The coordinate axes represent the responses of the N sensors. The components of the vector $\mathbf{p}$ are the outputs of the individual sensors and are functions of time. As time progresses, the tip of $\mathbf{p}$ then sweeps out a curve as shown in the figure. Due to obvious limitations, our illustrations can show at most $N=3$ and will show sensor outputs as real. These limitations will not adversely affect the illustration of key concepts.
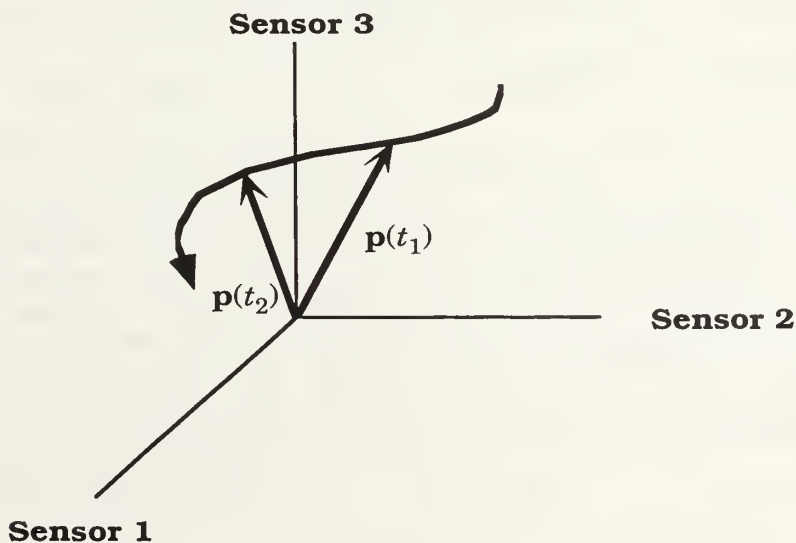
Figure 1: Behavior of signal vector

11

Now consider an example involving a single emitter ($d=1$; Figure 2). For this case, as time progresses, each component of **p** is multiplied by the *same* time-dependent phase factor. The (complex) *magnitude* of **p** changes, but its *direction* does not. Therefore, the "curve" swept out by **p** in this case is a *straight line* passing through the origin.

Sensor 3

$\mathbf{p}(t_2)$

$\mathbf{p}(t_1)$

Sensor 2

Sensor 1
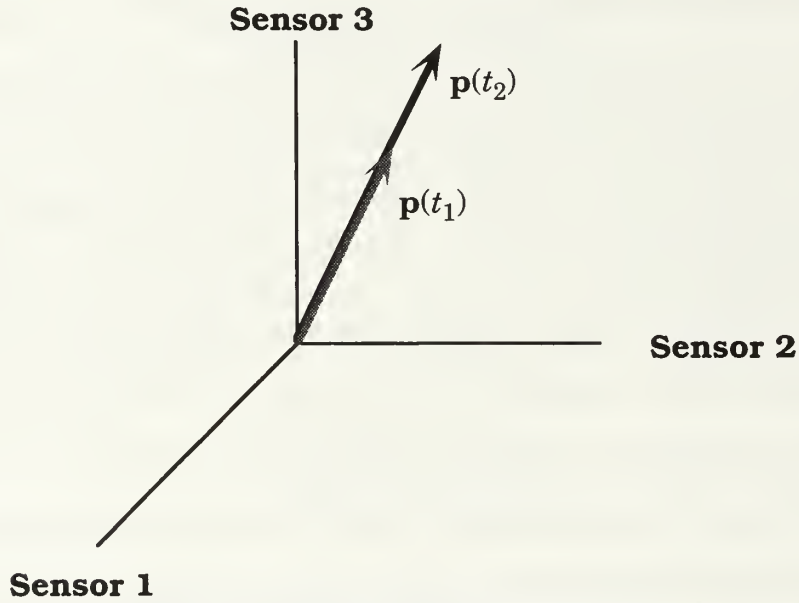
Figure 2: Signal Subspace (d=1)

Next consider an example involving two emitters (d=2) at angles θ_1 and θ_2 (Figure 3). For this case, **p** is the vector sum of contributions from the individual signals; specifically,

$$\mathbf{p} = s_1(t)\mathbf{a}(\theta_1) + s_2(t)\mathbf{a}(\theta_2). \tag{6}$$

These contributions $s_i(t)\mathbf{a}(\theta_i)$ are vectors whose magnitude varies with time, but whose direction is fixed by $\mathbf{a}(\theta_i)$. Since the two vectors are multiplied by *different* time-varying phase factors $s_i(t)=S_i\exp(j\omega t)$ (provided that the slowly varying complex amplitudes S_i are not perfectly correlated), their sum **p** sweeps out a curve which is confined to a *plane* passing through the origin.

12

In general, for d emitters, the tip of the received signal vector **p** sweeps out a curve which is confined to a d-dimensional subspace of $\mathbb{C}^N$. This subspace is known as the *signal subspace*. Intuitively, then, the *number* of emitters could be determined by measuring the dimension of the signal subspace. We will show later how this can be done.
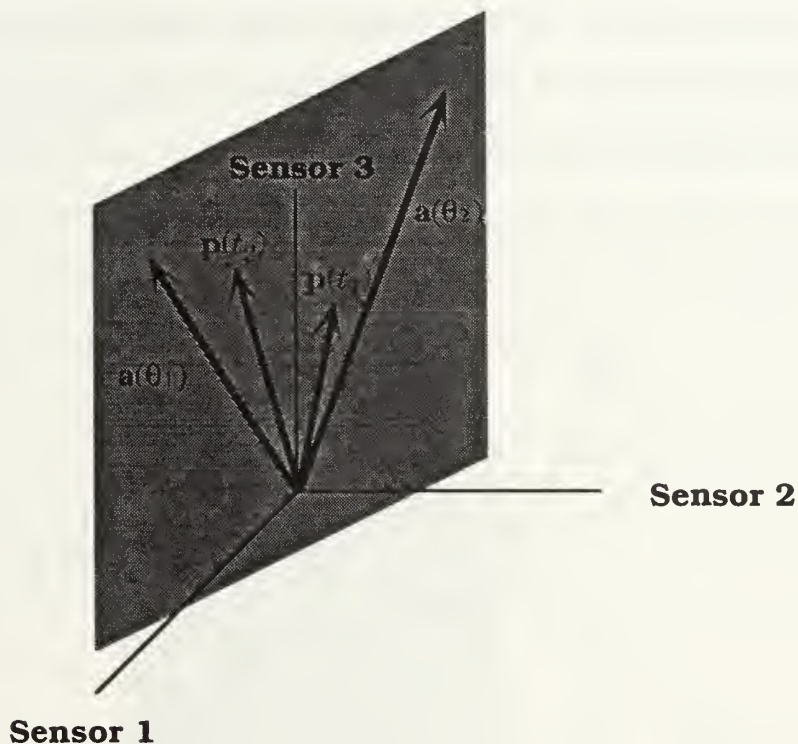
Figure 3: Signal Subspace (d=2)

Array Manifold. Figure 4 illustrates an array manifold, *i.e.,* the locus of the array response vectors $\mathbf{a}(\theta)$ for all possible values of θ. Note that, by definition, **a** is independent of time, so that time does not participate in this illustration. In practice, it is not necessary to have an analytical expression for $\mathbf{a}(\theta)$; we can instead determine it experimentally at a finite number of points, store the results, and recall them when desired (interpolating when necessary).

It may happen that the array manifold "runs over itself" (*i.e.*, the mapping $\mathbf{a}(\theta)$ from the interval 0 to 2π into $\mathbb{C}^N$ is not one-to-one). In such a case, the array is said to have an *ambiguity*. Such an ambiguity is not the only kind possible. For example, when the **a** vectors corresponding to 3 different DOAs lie in a single plane, the array also has an ambiguity (for reasons which may not be obvious at this point). In general, when the **a** vectors corresponding to $n+1$ different DOAs lie in a subspace of dimension n or less, the array is said to have a *rank n* ambiguity.

Sensor 3

$\mathbf{a}(\theta_2)$

$\mathbf{a}(\theta_1)$

Sensor 2

Sensor 1
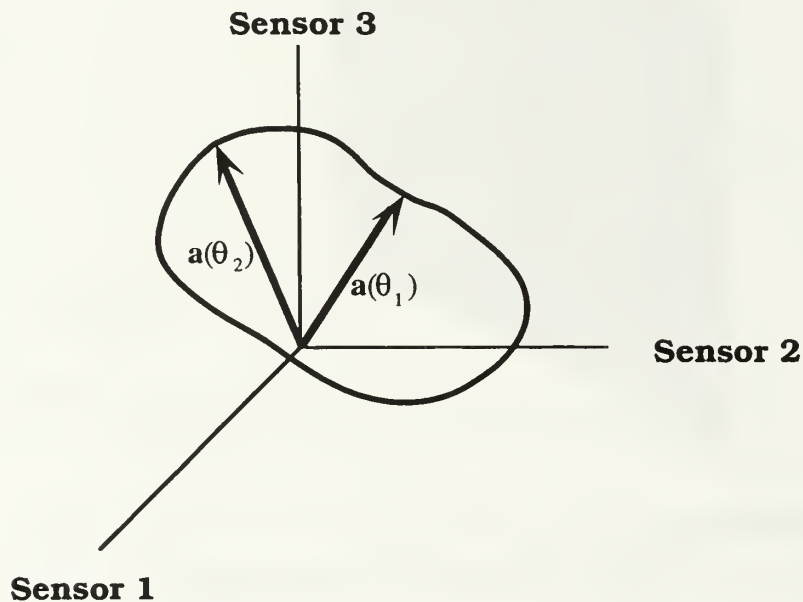
Figure 4: Array manifold

DOA Determination. For the case of one emitter, it is clear that the array response **a** corresponding to the emitter DOA lies in the (1-dimensional) signal subspace illustrated in Figure 2. In order to determine the DOA, we would observe the behavior of the signal vector **p** (if no noise were present) to determine the signal subspace and find the single unit vector that spans the subspace. This unit vector represents a point on the array manifold corresponding to the angle of the emitter. We would then invert the

mapping $\mathbf{a}(\theta)$ (which is one-to-one unless the array has an ambiguity) to determine the DOA θ.

Now consider the case of two emitters and recall that the signal vector $\mathbf{p}$ is the sum of (vector) contributions from the individual emitters (6). At any time t, these contributions are scalar multiples of the $\mathbf{a}$ vectors corresponding to the two emitter DOAs. Thus, the signal subspace is spanned by two vectors $\mathbf{a}(\theta_1)$ and $\mathbf{a}(\theta_2)$ which correspond to the points where the array manifold intersects the signal subspace (Figure 5). If the array has no ambiguities, there is no third $\mathbf{a}$ vector that lies in the subspace. Thus, just as in the case of one emitter, we can invert the $\mathbf{a}(\theta)$ mapping provided by the array manifold to determine the DOAs (Figure 5).

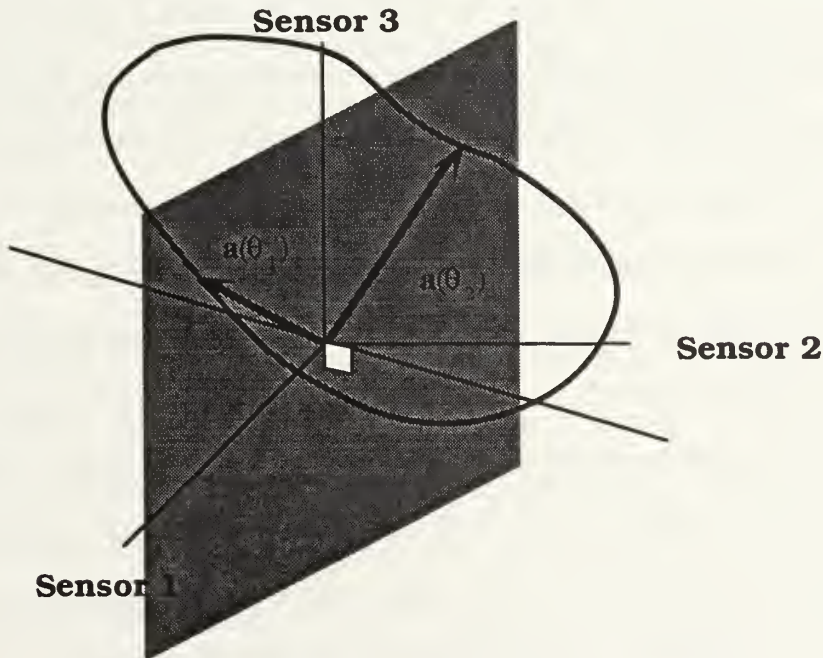**Figure 5: DOA Determination for 2 emitters**

In general, we observe the data vector $\mathbf{p}$, determine the signal subspace, find its intersection (d different $\mathbf{a}$ vectors) with the array manifold, and invert the mapping $\mathbf{a}(\theta)$ to estimate the DOAs of the emitters. It is apparent that, in general, this method requires the number of emitters d to

be fewer than the number of array elements N (if $d \geq N$, the entire array manifold may lie within the signal subspace). Clearly, if the array manifold is such that the **a** vectors corresponding to the emitter DOAs are not linearly independent (array ambiguity), the signal subspace dimension is less than the number of emitters. In such a case, the method described above fails to give the correct number of emitters and fails to identify one or more of the emitter DOAs. Such ambiguities can often be avoided by proper array design (although sometimes physical constraints, such as in line arrays, preclude such design).

Multipath. It is possible for the emissions from a single emitter to arrive by two or more different paths (*e.g.,* as a result of reflection from the water surface, in the sonar case). To illustrate the effect of such a situation, we consider the case of an array receiving signals from one emitter via two different DOAs. In such a case, the two signals will exhibit perfect temporal correlation (at least in theory). Recall that it is the *independent* variation with time of the array output due to individual signals from different DOAs that causes the signal vector to sweep out a two-dimensional subspace (Figure 3). In the multipath case, however, the array no longer responds *independently* to signals received from the two DOAs: the signal subspace is *one-dimensional*. In addition, note that this signal subspace is *not* spanned by any combination of vectors in the array manifold. Thus, the geometric approach is incapable of dealing with *perfectly coherent* multipath. Fortunately, such multipath is rarely, if ever, observed in real life. However, the performance of most geometrically-based algorithms degrades rapidly as the correlation between emitters (or multipath arrivals) approaches 1.

Noise. The above discussion assumes that no noise is present. With noise present, the signal-plus-noise vector **p** sweeps out a curve that no

longer lies in the signal subspace. Thus, the simple techniques described are not valid if noise is present.

Essentially, the technique described above for noise-free conditions must be modified as follows. For simplicity, we will assume that the noise is spatially isotropic and uncorrelated, so that (2) becomes

$$\mathbf{R}_{\mathrm{p}} = \mathbf{A}\mathbf{R}_{\mathrm{s}}\mathbf{A}^H + \sigma^2\mathbf{I}_N,$$

where $\mathbf{I}_N$ is the $N{\times}N$ identity matrix and the covariance matrices $\mathbf{R}_{\mathrm{s}}$ and $\mathbf{R}_{\mathrm{p}}$ represent *theoretical*, not *estimated* statistics. We now consider the following eigenvalue problem:

$$\mathbf{R}_{\mathrm{p}}\mathbf{e} = \lambda\mathbf{e}.$$

Since $\mathbf{R}_{\mathrm{p}}$ is Hermitian, the eigenvalues are real and the associated eigenvectors may be selected to be orthonormal [Ref. 33]. Then,

$$\begin{aligned}
0 &= \det\!\left[\mathbf{R}_{\mathrm{p}} - \lambda\mathbf{I}_N\right] \\
&= \det\!\left[\mathbf{A}\mathbf{R}_{\mathrm{s}}\mathbf{A}^H - \left(\lambda - \sigma^2\right)\mathbf{I}_N\right].
\end{aligned} \tag{7}$$

Per the definition of the $N{\times}d$ matrix $\mathbf{A}$, the columns of $\mathbf{A}$ are the $\mathbf{a}$ vectors corresponding to the d emitters. As mentioned above, if the array has no ambiguities, these $\mathbf{a}$ vectors are linearly independent and therefore $\mathbf{A}$ has full (column) rank d. The elements $R_s(i,j)$ of $\mathbf{R}_{\mathrm{s}}$ have the form $r_{ij}S_iS_j{}^*$, where r_{ij} is a correlation coefficient between the ith and jth signals and S_i represents the (complex) signal amplitude (not a function of time in this case) of the ith signal. Thus, the $d{\times}d$ matrix $\mathbf{R}_{\mathrm{s}}$ has full rank d unless one or more pairs of emitters are perfectly correlated (in which case $r_{ij}{=}1$ for some i, j and therefore the ith and jth columns are linearly dependent). Thus, assuming no array ambiguities and less than perfectly correlated emitters, the first term

in equation (7) is an $N{\times}N$ matrix of rank d. That term therefore has d non-zero eigenvalues v_i and $N{-}d$ zero eigenvalues. Since the eigenvectors of this term are also eigenvectors of the second term (identity matrix), the eigenvalues of the sum of the two terms in equation (7) are the sums of the respective eigenvalues; *i.e.*, the eigenvalues of $\mathbf{R_p}$ are

$$\{\lambda_i\} = \{v_1 + \sigma^2, \ldots, v_d + \sigma^2, \sigma^2, \ldots, \sigma^2\}.$$

The eigendecomposition of $\mathbf{R_p}$ may thus be expressed as

$$\begin{aligned}\mathbf{R_p} &= \mathbf{E}\Lambda\mathbf{E}^H \\ &= \mathbf{E_S}N_S\mathbf{E_S}^H + \sigma^2\mathbf{I}_N,\end{aligned}$$

where $\mathbf{E}$ is the matrix of eigenvectors, $\Lambda = \mathrm{diag}(\lambda_i)$, $\mathbf{E_S}$ contains the columns of $\mathbf{E}$ corresponding to non-zero eigenvalues of $\mathbf{AR_sA}^H$, and $N_S = \mathrm{diag}(v_i)$. Now consider the equality

$$\mathbf{AR_SA}^H = \mathbf{E_S}N_S\mathbf{E_S}^H. \tag{8}$$

Obviously, both the $d{\times}d$ diagonal matrix N_S and the $N{\times}d$ matrix $\mathbf{E_S}$ have rank d. Thus we see that the right hand side of (8) consists of a $N{\times}N$ matrix with rank d, each of whose columns is a linear combination of the d columns of $\mathbf{E_S}$. Therefore, the N columns of the right hand side must span the same subspace as the d columns of $\mathbf{E_S}$. Similarly, the columns of the left hand side of (8) must span the same subspace as the d columns of $\mathbf{A}$. Consequently, the columns of $\mathbf{E_S}$ must span the signal subspace (the subspace spanned by the columns of $\mathbf{A}$). In the presence of noise, then, the signal subspace may be determined by performing an eigendecomposition. The $N{-}d$ eigenvectors corresponding to the zero eigenvalues of $\mathbf{AR_sA}^H$ span what is referred to as the *noise subspace* (the orthogonal complement to the signal subspace). In the case where the noise is not isotropic and spatially uncorrelated, a *generalized*

eigendecomposition [Ref. 23] must be used; such a decomposition requires that an estimate of the noise covariance be available. The existence of an estimate of the noise covariance will not be assumed in the data analysis to follow, so we will not address this generalized eigendecomposition further. Obviously, there is some price to be paid for not incorporating the structure of the noise covariance in our method; we expect this price to increase as signal-to-noise ratio decreases.

In the real world, the covariance matrices are never known exactly, but must be estimated from observations. In the data analysis to be presented later, the following estimate of the covariance matrix will be used:

$$\hat{\mathbf{R}}_p = \mathbf{P}\mathbf{P}^H/L,$$

where L is the number of observations and $\mathbf{P}$ is an $N{\times}L$ matrix whose columns are observations of the received signal $\mathbf{p}$ at successive times; *i.e.*,

$$\mathbf{P} = \begin{bmatrix} \mathbf{p}(t_1) \mid \mathbf{p}(t_2) \mid \cdots \mid \mathbf{p}(t_L) \end{bmatrix}.$$

Because of estimation errors, the $N{-}d$ noise eigenvalues of this estimated covariance matrix will not have exactly the same value σ^2, so that even the number of emitters d cannot be estimated with certainty. For the purpose of the present discussion, however, we assume that d is known. Estimates of the signal subspace may then be obtained via the familiar Linear Least Squares and Maximum Likelihood techniques [Ref. 23]. For the simple case of Gaussian noise, these techniques give the same result, but one which is not computationally feasible in most practical situations (since both involve a global minimization over a space with dimension equal to the number of emitters). The MUSIC algorithm discussed in the sequel arose out of the need to reduce computational complexity.

Estimating the Subspace Dimension. In an *optimal* estimator, the problem of estimating the subspace dimension cannot be decoupled from that of estimating the subspace itself. However, in the interest of reducing computational load, we can estimate the dimension separately. This feature of the MUSIC algorithm therefore causes it to be suboptimal.

Estimating the Signal Parameters. As mentioned earlier, in the presence of noise, we can no longer depend on precise intersections between the signal subspace determined from the estimated covariance matrix $\hat{\mathbf{R}}_p$ and the array response vectors corresponding to the signal DOAs. To estimate these DOAs, we must therefore determine those **a** vectors which are "closest" (in some sense) to the signal subspace. There are several possible methods for doing this; we consider only the simplest method (Conventional MUSIC) here.

Recall from the earlier discussion that when the theoretical (*i.e.*, not estimated) covariance matrix $\mathbf{R}_p$ is used to determine the signal and noise subspaces, the array response vectors corresponding to the signal DOAs span the signal subspace and are orthogonal to the noise subspace. Thus, the squared length of the projection of an **a** vector onto the noise subspace, given by

$$\text{Length squared} = \mathbf{a}^H(\theta)\mathbf{E}_N\mathbf{E}_N^H\mathbf{a}(\theta),$$

will be zero when θ is one of the emitter DOAs. However, because of estimation errors (as well as because of inaccuracies in the signal model used to determine $\mathbf{a}(\theta)$), when the estimated covariance matrix $\hat{\mathbf{R}}_p$ is used to determine the signal and noise subspaces (*i.e.*, to determine $\mathbf{E}_N$), this quantity will generally not be zero for any **a**. We must therefore search the array

manifold for the set of d array response vectors which result in the lowest value for the quantity. An alternative method for accomplishing this is to define the function

$$P_M(\theta) = \frac{1}{\mathbf{a}^H(\theta)\mathbf{E}_N\mathbf{E}_N^H\mathbf{a}(\theta)}. \tag{9}$$

The estimates of the signal DOAs then correspond to the peaks of this function. Although this function is similar in some respects to beamformer output power functions such as that in (5), the peak heights of this function do not necessarily provide any information about the power in their respective components.

B. HIGHER-ORDER STATISTICS

In recent years, there has been increasing interest in the use of higher-order (*i.e.,* order greater than 2) statistics in signal processing. One reason for this interest is that the statistics known as *cumulants* are identically zero for Gaussian random variables, provided that the order of the cumulant is greater than 2. Intuitively, we would expect that, in situations where the noise is Gaussian but the signal is not, cumulant-based methods offer potentially large performance improvements over conventional methods based on second-order statistics, by removing the noise without affecting the signal. A detailed treatment of higher-order statistics is beyond the scope of this dissertation; for the purposes of this discussion, a brief consideration of the 4th-order cumulant will suffice. Broader treatments of the topic (including the material in the sequel) may be found in articles by Shiryaev [Ref. 34], Brillinger [Ref. 35], and Brillinger and Rosenblatt [Ref. 36]; tutorial articles by Nikias and Raghuveer [Ref. 37] and Mendel [Ref. 38]; and the recent textbook by Nikias and Petropulu [Ref. 39].

The *joint characteristic function* Φ of a set $\{x_1, x_2,..., x_n\}$ of n real random variables is defined [Ref. 25] by

$$\Phi(\omega_1, \omega_2,..., \omega_n) = E\left\{\exp\left[j(\omega_1 x_1 + \omega_2 x_2 + \cdots + \omega_n x_n)\right]\right\},$$

where E denotes statistical expectation, as before. The form of this function obtained by making the substitution $s_i = j\omega_i$ is known as the *moment-generating function*; the moments of the x_i can be obtained from the coefficients of the Taylor expansion of the moment-generating function about $s_i = 0$. The *second characteristic function* Ψ of these same random variables is defined as $\Psi = \ln \Phi$. The *joint cumulants* of order $r = k_1 + k_2 + \cdots + k_n$ of these random variables are defined [Ref. 25] as

$$Cum\left[x_1^{k_1}, x_2^{k_2},..., x_n^{k_n}\right] = (-j)^r \left.\frac{\partial^r \Psi(\omega_1, \omega_2,..., \omega_n)}{\partial \omega_1^{k_1} \partial \omega_2^{k_2} \cdots \partial \omega_n^{k_n}}\right|_{\omega_1 = \omega_2 = ... = \omega_n = 0}, \qquad (10)$$

i.e., the coefficients of the Taylor expansion of Ψ about $\omega_i = 0$. For the 4th-order cumulant of zero-mean real random variables x_i, it can be shown [Refs. 34, 39] that (10) reduces to

$$\begin{aligned} Cum(x_1, x_2, x_3, x_4) = &\; E[x_1 x_2 x_3 x_4] - E[x_1 x_2] \cdot E[x_3 x_4] \\ &- E[x_1 x_3] \cdot E[x_2 x_4] - E[x_1 x_4] \cdot E[x_2 x_3]. \end{aligned} \qquad (11)$$

It may further be shown [Ref. 25] that, if the x_i are jointly Gaussian, the 4th order moment is given by

$$E[x_1 x_2 x_3 x_4] = E[x_1 x_2] \cdot E[x_3 x_4] + E[x_1 x_3] \cdot E[x_2 x_4] + E[x_1 x_4] \cdot E[x_2 x_3]; \qquad (12)$$

therefore the cumulant vanishes as claimed. For complex random variables, (11) takes the form [Ref. 40]

$$Cum(x_1, x_2^*, x_3, x_4^*) = E[x_1 x_2^* x_3 x_4^*] - E[x_1 x_2^*] \cdot E[x_3 x_4^*]$$
$$-E[x_1 x_3] \cdot E[x_2^* x_4^*] - E[x_1 x_4^*] \cdot E[x_2^* x_3] , \qquad (13)$$

where the third term is generally assumed to be zero due to the symmetry property between the real and imaginary parts of a stationary, bandpass, complex process [Ref. 41]. We will retain this term for generality.

A spatial 4th-order cumulant matrix $\mathbf{C}_4$ may be defined as follows:

$$\mathbf{C}_4 = Cum \left\{ \begin{bmatrix} p_1(t)p_1^*(t) \\ p_2(t)p_2^*(t) \\ \vdots \\ p_N(t)p_N^*(t) \end{bmatrix} [p_1(t)p_1^*(t), p_2(t)p_2^*(t), \cdots, p_N(t)p_N^*(t)] \right\}, \qquad (14)$$

where "*" denotes complex conjugate and the $p_i(t)$ are sensor signals (complex pre-envelopes) at each of N sensors in an array. This definition differs from the one used by Nikias and Petropolu [Ref. 39], but was selected so that $\mathbf{C}_4$ is Hermitian. By substituting (11) into (14), and using vector notation, we obtain

$$\mathbf{C}_4 = E\left\{ (\mathbf{p} \circ \mathbf{p}^*)(\mathbf{p} \circ \mathbf{p}^*)^H \right\} - E\{\mathbf{p} \circ \mathbf{p}^*\} E\left\{ (\mathbf{p} \circ \mathbf{p}^*)^H \right\}$$
$$-E\{\mathbf{p}\mathbf{p}^H\} \circ E\{\mathbf{p}^*\mathbf{p}^T\} - E\{\mathbf{p}\mathbf{p}^T\} \circ E\{\mathbf{p}^*\mathbf{p}^H\} , \qquad (15)$$

where $\circ$ denotes the element-by-element product of the vectors and superscript T indicates (non-conjugate) matrix transpose. The fourth term of (15) is generally assumed to be zero due to the symmetry property discussed in conjunction with (13) but will be retained for generality. Substituting the signal model of equation (1) (for the case of a single emitter) into (15) gives

$$\mathbf{C}_4 = E\left\{ (\mathbf{a}s \circ \mathbf{a}^* s^*)(\mathbf{a}s \circ \mathbf{a}^* s^*)^H \right\} - E\{\mathbf{a}s \circ \mathbf{a}^* s^*\} E\left\{ (\mathbf{a}s \circ \mathbf{a}^* s^*)^H \right\}$$
$$-E\{\mathbf{a}s s^* \mathbf{a}^H\} \circ E\{\mathbf{a}^* s^* s \mathbf{a}^T\} - E\{\mathbf{a}s s \mathbf{a}^T\} \circ E\{\mathbf{a}^* s^* s^* \mathbf{a}^H\}$$

23

provided that the signal and noise are independent (the single-emitter assumption is made here for notational convenience and will also be made during the actual data analysis in the sequel). Since **a** is deterministic, it may be factored out of the expectation operators, and we obtain, after some algebra

$$\mathbf{C}_4 = \gamma\left(\mathbf{a} \circ \mathbf{a}^*\right)\left(\mathbf{a} \circ \mathbf{a}^*\right)^H, \tag{16}$$

where

$$\gamma = \mathrm{Cum}\left\{s(t), s^*(t), s(t), s^*(t)\right\}$$

is the kurtosis measure of the (single) emitter signal $s(t)$ and **a** is the array response vector corresponding to the location of the emitter.

The structure of $\mathbf{C}_4$ is therefore identical to that of the covariance matrix defined in (2), except that: 1) the noise covariance vanishes due to the properties of the 4th-order cumulant; 2) the array response vector **a** is replaced by $\mathbf{a} \circ \mathbf{a}^*$, which is real; and 3) $\mathbf{C}_4$ has rank 1 (see (16)) due to the assumption of a single emitter and is real. This structure allows the use of a modified version of the previously discussed MUSIC algorithm as follows:

- Form an estimate $\hat{\mathbf{C}}_4$ of the $\mathbf{C}_4$ matrix from the measured data using (15), with expectation operators replaced by time averages;

- Perform an eigendecomposition of $\hat{\mathbf{C}}_4$. Because it has rank 1, there will be (theoretically) a single non-zero eigenvalue.

- Select the eigenvector corresponding to the largest eigenvalue; as shown earlier (8), this eigenvector must span the same subspace as the **a** vector corresponding to the actual emitter location. The

remaining eigenvectors span the noise subspace and form the columns of $\mathbf{E_N}$.

- Form the function

$$P_M = \frac{1}{\left[\mathbf{a}(\theta) \circ \mathbf{a}*(\theta)\right]^H \mathbf{E_N E_N^H} \left[\mathbf{a}(\theta) \circ \mathbf{a}*(\theta)\right]};$$ (17)

the estimate for the emitter location corresponds to the peak of this function. This method can be easily generalized to the multiple-emitter scenario, provided that the signal subspace dimension is selected to correspond to the number of emitters. However, our experimental work with real data does not require this generalization.

Cumulant-based versions of the Bartlett and MVM methods also exist [Ref. 39], but these will not be used in the data analysis. It should also be noted that the form of the 4th-order cumulant appearing in (15) is a reduced form of that used by Porat and Friedlander [Ref. 20].

C. ACOUSTICS AND MODELING

1. Helmholtz Equation

Whereas in DOA estimation the received signals are assumed to be plane waves, in MFP the pressure field amplitude $p(r,z)$ in an underwater channel (see Figure 6) due to a narrowband emitter with center frequency ω is assumed to satisfy the Helmholtz equation [Ref. 42]

$$\frac{1}{r}\frac{\partial}{\partial r}\left[r\,\frac{\partial p(r,z)}{\partial r}\right] + \frac{\partial^2 p(r,z)}{\partial z^2} + k(r,z)^2 p(r,z) = 0,$$ (18)

where r is the range from the emitter to the observation point, z is the depth, and $k = \omega/c$ is the wavenumber. Cylindrical coordinates are used in (18)

because of the symmetry which exists when changes in sound speed in the azimuthal direction are negligible. The sequel will present an overview of methods for solving (18) numerically which are pertinent to this dissertation. In this section, it will be assumed that no observation noise is present.
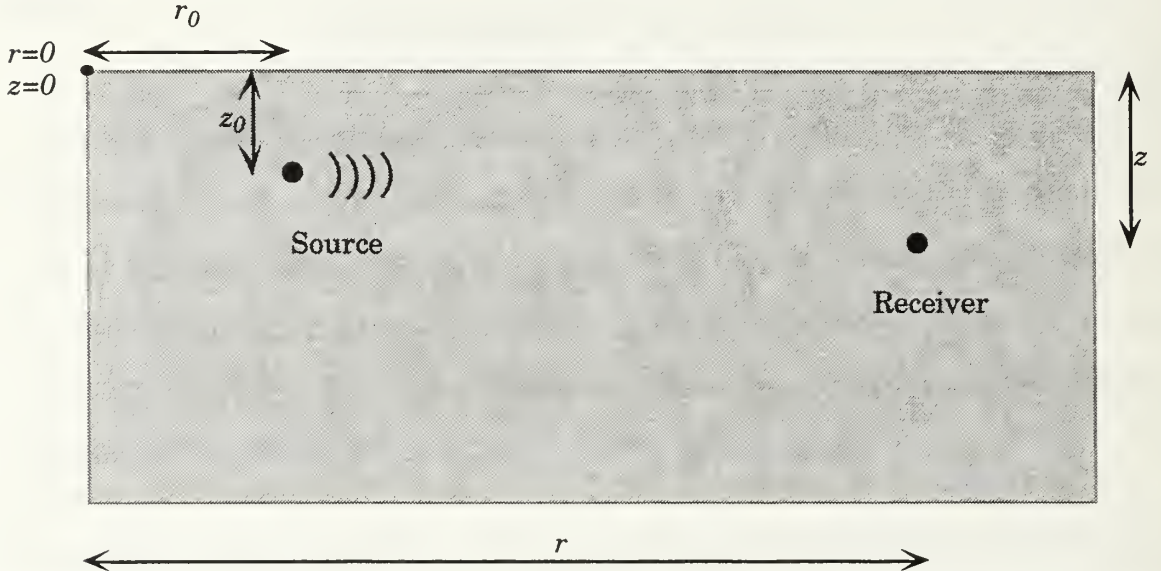

Figure 6: Generic Underwater Channel

2. Normal Mode Solution

In a channel where all properties (sound speed, water depth, bottom type, etc.) are independent of horizontal range, it is well known [Ref. 42] that the pressure field p at range r (relative to an arbitrary origin; see Figure 6) sufficiently far away from the emitter and at depth z may be expanded in terms of normal modes as follows:

$$p(r, z, t; r_0, z_0) = \sum_{m=1}^{\infty} \frac{A}{\sqrt{k_m(r - r_0)}} Z_m(z) Z_m(z_0) e^{j[\omega t - k_m(r - r_0)]}, \qquad (19)$$

where: z_0 and r_0 are the emitter depth and range, respectively; r is taken to be greater than r_0; A is a constant which depends on the emitter power; and the Z_m and k_m are the eigenfunctions and eigenvalues, respectively, of the ordinary differential equation

26

$$\frac{d^2 Z_m}{dz^2} + \left[\frac{\omega^2}{c^2(z)} - k_m^2 \right] Z_m = 0. \tag{20}$$

The boundary conditions for (20) depend on the acoustic properties of the surface (which is always assumed to be pressure-release; i.e., $p(z=0)=0$) and the bottom. Attenuation due to sediment and water column is incorporated, as is customary, via a small imaginary part in the k_m. Although the sum in (19) is over values of m from 1 to infinity, all modes for which m is greater than some integer M are attenuated enough to be ignored at the ranges of interest; such modes include the strongly bottom-interacting and evanescent modes. In the discussions to follow, we will ignore these modes and incorporate only the lowest M modes in our normal mode expressions. It should be noted that, in general (i.e., for range near zero), the expansion (19) is only approximate, since it only accounts for the discrete spectrum of the modal solution to the Helmholtz equation (18). This fact does not present a problem, however, because the contribution to the pressure field from the continuous spectrum is negligible at the ranges of interest in MFP/MMP. Numerous methods exist for implementing (19) on a computer (see, for example, [Ref. 43]). As is characteristic of solutions of boundary value problems such as (20), the Z_m are orthogonal with respect to the density function $\rho(z)$, i.e.,

$$\int_0^\infty \frac{1}{\rho(z)} Z_m(z) Z_n(z) dz = v_n \delta(m-n), \tag{21}$$

where

$$v_n = \int_0^\infty \frac{1}{\rho(z)} Z_n^2(z) dz$$

This orthogonality will prove useful later in the discussion of Matched-Mode Processing.

3. Adiabatic Approximation

As mentioned above, the normal mode expression (19) is strictly valid only in range-independent environments; nevertheless, it can be modified slightly to apply to a limited class of range-dependent environments. Whenever range dependence exists (due to a sloping bottom or change in sound speed profile, for example), it is clear that the Z_m and k_m must be functions of range. If the range dependence is relatively weak, it can be assumed that a mode does not exchange energy with other modes, but merely adapts itself to local environmental conditions. This assumption is known as the "adiabatic" approximation. In such a case, (20) is solved at each of the ranges of interest. The resulting Z_m and k_m are then functions of range, so that the pressure field can be expressed as

$$p(r,z,t;r_0,z_0) = \sum_{m=1}^{M} \frac{A}{\sqrt{k_m(r)(r-r_0)}} Z_m(r,z)Z_m(r_0,z_0)\exp\left[j\omega t - j\int_{r_0}^{r} k_m(r)dr\right]. \quad (22)$$

4. Coupled Mode Model

Due to the energy exchange between modes in a strongly range-dependent environment, the use of a normal-mode model in such an environment becomes more complex. For simplicity, we assume that horizontal refraction and azimuthal scattering are negligible (see [Ref. 44] for a fully three-dimensional treatment). As will be discussed in more detail later, this approximation is satisfactory for the acoustic environment addressed in the data analysis to follow [Ref. 19].

Mode coupling may be accounted for in a manner consistent with the notation used above by defining a range-dependent mode amplitude $A_m(r)$

28

(*i.e.*, the complex constant A in (22) becomes a function of both range and mode number m) [Ref. 45]. The pressure field is then given by

$$p(r, z, t; r_0, z_0) = \sum_{m=1}^{M} \frac{A_m(r; r_0, z_0)}{\sqrt{k_m(r)(r-r_0)}} Z_m(r, z) Z_m(r_0, z_0) \exp\left[j\omega t - j\int_{r_0}^{r} k_m(r)dr \right].(23)$$

In this expression, all coupling between modes is accounted for by the A_m (*i.e.*, each A_m depends on the mode amplitudes and phases of all other modes along the propagation path). The Broadband Coupled Mode model developed by Chiu *et al.* [Ref. 19] has demonstrated high accuracy in predicting the modal structure observed in the Barents Sea Polar Front Experiment and will be used for all data analysis in the sequel.

D. MATCHED-FIELD AND MATCHED-MODE PROCESSING

A good overview of this topic may be found in the textbook by Tolstoy [Ref. 46]. Only background material pertinent to the later data analysis (along with some preliminary material) will be presented here.

1. Motivation

Several limitations in applying DOA estimation techniques to the underwater acoustic localization problem arise from the inability of the simple plane-wave signal model to describe the acoustic field adequately. In this section, we describe these limitations, which provide the motivation for study of MFP/MMP.

a. Ability to determine target parameters

Because of the assumption that the received signal is a plane wave, the only degree of freedom in the array response vector is DOA. Therefore, DOA estimation is inherently incapable of providing any other information. In particular, it gives no range information, which in military

applications is of vital interest (although it should be pointed out that it is possible to determine range by observing DOA information *over time*, provided that certain assumptions concerning target motion are valid; see [Ref. 47]).

b.   *Estimation error*

Since the speed of sound in seawater is a function of position, the sound "rays" (*i.e.*, paths normal to the surfaces of constant phase) are curved. Consequently, the DOA estimates will, in general, be different from the actual directions of the emitters. In many practical situations, the receiving array has no depth extent (*e.g.*, a horizontal line array) and the ocean may be considered to be horizontally stratified (*i.e.*, speed of propagation is a function primarily of depth). In such situations, the plane wave signal model is relatively accurate. Even in such cases, the DOA estimates will often be significantly in error due to reflection of sound energy from boundaries (surface and bottom).

c.   *Loss of gain*

We have noted earlier that the Bartlett beamformer results in the highest output SNR, provided that the noise is spatially homogeneous. Essentially, this feature is due to the fact that the signals from different receive array elements add constructively (because the beamformer introduces phase shifts to account for the shape of the wavefront) while the noise components do not. In an underwater acoustic channel, however, the wavefronts may not be planar (particularly in the vertical direction), so that the signals from the array elements will no longer be added perfectly constructively (since the beamformer assumes the wavefront is planar when it actually is not). Consequently, the gain of the beamformer will be lower than when the incoming signal is a plane wave.

d. *Inability to resolve multipath arrivals*

As mentioned earlier, many eigenstructure-based methods (including MUSIC) are unable to handle signals from multiple highly correlated emitters. Reflections from boundaries in the underwater acoustic problem can often result in the same signal arriving at the receiver from multiple directions. This situation is equivalent to the presence of multiple, highly correlated emitters; thus, MUSIC and similar methods break down in such a situation.

2. Generalization of array processing algorithms

a. *Matched-Field Processing (MFP)*

For the case of a single signal, (1) becomes

$$\mathbf{p} = \mathbf{a}s(t) + \mathbf{n}. \tag{24}$$

We can use (23) to express the pressure at a receiving array consisting of a set of N vertically-aligned hydrophones at depths $\{z_1, z_2, ..., z_N\}$ in the form (24) if we identify

$$\mathbf{p} = \begin{bmatrix} p(r, z_1, t) \\ p(r, z_2, t) \\ \vdots \\ p(r, z_N, t) \end{bmatrix} \tag{25}$$

and

$$\mathbf{a} = \sum_{m=1}^{M} \frac{A_m(r)}{\sqrt{k_m(r)(r - r_0)}} \mathbf{Z}_m(r) Z_m(r_0, z_0) \exp\left[-j \int_{r_0}^{r} k_m(r) dr\right], \tag{26}$$

where $\exp(j\omega t) = s(t)$ and $\mathbf{Z}_m(r) = [Z_m(r, z_1), Z_m(r, z_2), ..., Z_m(r, z_N)]^T$. The array response vector $\mathbf{a}$ is now a function of emitter range r_0 and depth z_0 rather than azimuth, as in DOA estimation. The $\mathbf{a}(r_0, z_0)$ are obtained by calculating

the pressure field seen at the receive array using an appropriate propagation model, for every possible (r_0, z_0) combination of interest. In the previous discussions on DOA estimation, no assumptions were made concerning the form of **a**. Furthermore, the dependence of **a** on azimuth alone was for the purposes of illustration only, and is not required for the DOA estimation techniques to be valid. Therefore, the algorithms discussed above in the context of DOA estimation may be used in MFP as well [Refs. 3, 7]. It should be noted that MFP does not require that the acoustic field be expressed in terms of normal modes; the above analysis is valid for other types of propagation models as well.

The well-known principle of acoustic reciprocity (see, *e.g.*, [Ref. 48]) is very useful in minimizing the computations required to generate the array manifold. This principle states that, under a set of reasonable assumptions, the acoustic pressure at a location (r, z) generated by a simple source at location (r_0, z_0) is the same as the acoustic pressure at location (r_0, z_0) generated by that same source at location (r, z). In MFP, the construction of the array manifold requires that the field at a known receiver location (r, z) be computed for every possible emitter location (r_0, z_0), whereas one run of a propagation model will generally produce the acoustic field at every possible receiver location due to an emitter at a known, fixed location. Thus, it may be seen that this principle of acoustic reciprocity allows construction of one component (corresponding to one element of the receive array) of the array manifold with a single run of a propagation model. The total number of runs required will be the same as the number of elements in the receive array. Clearly, this approach allows huge savings in computation compared to a "brute force" approach which performs one run of a propagation model for each possible source location.

The procedure for MFP may be outlined as follows:

- Determine the pre-envelopes of the received (real) signals at each receive hydrophone. Use these pre-envelopes to generate an estimate (using time averages instead of statistical expectations) of the covariance matrix $\mathbf{R_p}$ (or the 4th order cumulant matrix $\mathbf{C_4}$);

- Using a suitable propagation model and invoking the principle of acoustic reciprocity, generate the array manifold vectors $\mathbf{a}(r_0, z_0)$ (which in the context of MFP/MMP are generally called *replica fields*) for values of (r_0, z_0) on a suitable grid;

- Generate the functions in equations (4) (Bartlett), (5) (MVM), (9) (MUSIC), or (17) (cumulant MUSIC), as desired. These will now be functions of two variables (r_0, z_0) rather than one (θ), *i.e.*,

$$B(r_0, z_0) = \mathbf{a}^H(r_0, z_0)\mathbf{R_p}\mathbf{a}(r_0, z_0) \text{ (Bartlett)}, \tag{27}$$

$$B(r_0, z_0) = \frac{1}{\mathbf{a}^H(r_0, z_0)\mathbf{R_p}^{-1}\mathbf{a}(r_0, z_0)} \text{ (MVM)}, \tag{28}$$

$$P_M(r_0, z_0) = \frac{1}{\mathbf{a}^H(r_0, z_0)\mathbf{E_N}\mathbf{E_N}^H\mathbf{a}(r_0, z_0)} \text{ (MUSIC)}, \tag{29}$$

$$P_M(r_0, z_0) = \frac{1}{\left[\mathbf{a}(r_0, z_0) \circ \mathbf{a}^*(r_0, z_0)\right]^H \mathbf{E_N}\mathbf{E_N}^H\left[\mathbf{a}(r_0, z_0) \circ \mathbf{a}^*(r_0, z_0)\right]} \text{ (Cumulant)}. \tag{30}$$

The estimated emitter locations are the (r_0, z_0) combinations for which these functions are maximized. In MFP/MMP, plots of these functions are generally referred to as *ambiguity surfaces*.

b.   *Matched-Mode Processing (MMP)*

MMP [Refs. 4, 49, 50, 51] requires the pressure field in the channel to be expanded in terms of normal modes. As will become clearer

later, it may be understood intuitively as a transformation of the observations from the space of individual hydrophones to the space of modal amplitudes. This transformation is known as *mode filtering*. As before, we will assume that an accurate representation of the field (23) requires only a finite number of terms M.

As with MFP, the pressure field is sampled with an N-element vertical array of identical elements at depths $\{z_1, z_2,...,z_N\}$, located a distance r relative to an arbitrary origin. The vector of received pressures (defined in (23) and (25)), without additive noise, may be expressed in matrix form as

$$\mathbf{p=Zu,} \qquad (31)$$

where

$$\mathbf{Z} = \begin{bmatrix} Z_1(r,z_1) & Z_2(r,z_1) & \cdots & Z_M(r,z_1) \\ Z_1(r,z_2) & Z_2(r,z_2) & & \vdots \\ \vdots & & \ddots & \vdots \\ Z_1(r,z_N) & \cdots & \cdots & Z_M(r,z_N) \end{bmatrix} \text{ and }$$

$$\mathbf{u} = \begin{bmatrix} u_1 & u_2 & \cdots & u_M \end{bmatrix}^T, \text{ with}$$

$$u_m(r,t) = \frac{A_m(r)}{\sqrt{k_m(r)(r-r_0)}} Z_m(r_0,z_0) \exp\left[j\omega t - j\int_{r_0}^{r} k_m(r)dr \right]. \qquad (32)$$

$\mathbf{Z}$ thus contains all information about the receiving array, while $\mathbf{u}$ contains all information about the location of the emitter relative to the receiver. Both $\mathbf{Z}$ and $\mathbf{u}$ contain information about the channel via the eigenfunctions Z_m, which are derived from normal mode analysis. An estimate $\hat{\mathbf{u}}$ of $\mathbf{u}$ may be obtained from (31) using either of two classes of methods.

The first class of methods regards estimation of $\hat{\mathbf{u}}$ from a purely mathematical perspective, namely, as a least-squares problem [Ref. 33],

either overdetermined ($N \geq M$) or underdetermined ($N < M$). In this problem, $\hat{\mathbf{u}}$ is selected to minimize the quantity

$$\|\mathbf{Z}\hat{\mathbf{u}} - \mathbf{p}\|_2^2, \tag{33}$$

the squared Euclidean norm of the residual ($\mathbf{Z}\hat{\mathbf{u}} - \mathbf{p}$). In the overdetermined case, assuming that $\mathbf{Z}$ has full rank, the solution $\hat{\mathbf{u}}$ is unique. In that case, the selection of a suitable method is based on considerations of numerical stability and computational complexity. If the problem is underdetermined (as is the case with the data to be analyzed in this dissertation) or $\mathbf{Z}$ is rank-deficient, there is an infinitude of vectors $\hat{\mathbf{u}}$ which minimize (33). Two subclasses of least-squares methods exist in this case: those which produce a solution $\hat{\mathbf{u}}$ with minimum norm (such as the pseudo-inverse method discussed below) and those which do not (such as certain versions of the QR factorization method). Methods in the latter subclass give solutions with significantly greater sensitivity when $\mathbf{p}$ is contaminated by observation noise. We will consider only the pseudo-inverse method in this dissertation.

The singular value decomposition (SVD) of Z is given by [Ref. 33]

$$\mathbf{U}^H \mathbf{Z} \mathbf{V} = \mathrm{diag}\left(\sigma_1, \sigma_2, \ldots, \sigma_p\right)$$

$$= \begin{bmatrix} \sigma_1 & & & \vdots \\ & \ddots & & \vdots & 0 \\ & & \sigma_N & \vdots \end{bmatrix} = \Sigma$$

where $\mathbf{U}$ and $\mathbf{V}$ are $N{\times}N$ and $M{\times}M$ unitary matrices respectively, $p=\min(M,N)$, and the σ_i are the (real and non-negative) singular values (some of the σ_i will be zero if $\mathbf{Z}$ is rank-deficient). Note that the matrix partition

shown assumes $N \leq M$; the partition when $N > M$ is analogous. The pseudoinverse $\mathbf{Z}^+$ of $\mathbf{Z}$ is defined as

$$\mathbf{Z}^+ = \mathbf{V}\Sigma^+\mathbf{U}^H,$$

where

$$\Sigma^+ = \text{diag}\left(\frac{1}{\sigma_1}, \ldots, \frac{1}{\sigma_R}, 0, \ldots, 0\right) \tag{34}$$

and $R = \text{rank}(\mathbf{Z})$. The minimum-norm solution of (31) can be expressed as

$$\hat{\mathbf{u}} = \mathbf{Z}^+\mathbf{p}. \tag{35}$$

Obviously, the expression (30) is very sensitive to the presence of small but non-zero singular values (due, *e.g.*, to roundoff error). This phenomenon may be satisfactorily dealt with by treating all singular values on the order of machine precision (or smaller) as zero. As is well known, if $N \geq M$ and $\mathbf{Z}$ has full rank, the unique least-squares solution is given by

$$\hat{\mathbf{u}} = \mathbf{Z}^+\mathbf{p} = \left(\mathbf{Z}^H\mathbf{Z}\right)^{-1}\mathbf{Z}^H\mathbf{p}.$$

This method of modal decomposition is referred to by Yang [Ref. 52] as the "Eigenvector Method". Obviously, modes which are so poorly sampled by the receive array that the corresponding columns of $\mathbf{Z}$ are nearly linearly dependent cannot be resolved using this approach.

As mentioned earlier, the analysis to follow does not assume the existence of an estimate of the noise covariance. It is worth noting that, when $\mathbf{p}$ is contaminated by observation noise with *known* covariance (*i.e.*, known, except possibly for a constant multiplicative factor), $\hat{\mathbf{u}}$ should be determined via the *generalized least-squares* method [Ref. 33] in order to ensure that

undue weight is not given to data from hydrophones with high levels of observation noise. Since this method will not be used in our analysis, it will not be discussed further.

The second class of methods (see, for example, [Ref. 51]) for estimating $\hat{\mathbf{u}}$ regards the problem from a more physical perspective; *i.e.*, it exploits the orthogonality property of the mode functions (columns of $\mathbf{Z}$) (21). In (21), if the spacing of hydrophones is sufficiently dense, the integral may be replaced by a sum without significant loss of accuracy. Furthermore, within the water column, the density ρ is approximately independent of depth. Thus, the columns of $\mathbf{Z}$ are approximately orthogonal, at least for the lower modes (*i.e.*, for those modes which are well sampled by the receiver depths z_i), *i.e.*,

$$\mathbf{Z}^H \mathbf{Z} \approx \frac{\rho}{\Delta z} \operatorname{diag}(v_1, v_2, \ldots, v_M),$$

where Δz is the spacing of the vertical grid on which the mode function is evaluated. To obtain an estimate of $\mathbf{u}$, we premultiply (31) by $\mathbf{Z}^H$

$$\mathbf{Z}^H \mathbf{p} = \mathbf{Z}^H \mathbf{Z} \mathbf{u}$$
$$\approx \frac{\rho}{\Delta z} \operatorname{diag}(v_1, v_2, \ldots v_M) \cdot \mathbf{u}.$$

We may thus take the estimate of $\mathbf{u}$ to be

$$\hat{\mathbf{u}} = \frac{\Delta z}{\rho} \operatorname{diag}\left(\frac{1}{v_1}, \frac{1}{v_2}, \cdots, \frac{1}{v_M}\right) \mathbf{Z}^H \mathbf{p}. \tag{36}$$

This method of estimating $\mathbf{u}$, which we will refer to as the *projection method*, is obviously very similar mathematically to the pseudoinverse method. Because of the mode orthogonality assumption, only modal amplitudes

corresponding to those columns of **Z** which form a (nearly) mutually orthogonal set may be accurately estimated.

When observation noise is present, (31) becomes

$$\mathbf{p} = \mathbf{Z}\mathbf{u} + \mathbf{n}.$$

As mentioned earlier, because we do not assume that an estimate for the noise covariance is available, the presence of this observation noise does not affect how we estimate **u** (although, of course, the *value* of the estimate will be affected). Using the pseudoinverse method to estimate **u**, we obtain

$$\begin{aligned}
\hat{\mathbf{u}} &= \mathbf{Z}^{+}\mathbf{p} \\
&= \mathbf{Z}^{+}\mathbf{Z}\mathbf{u} + \mathbf{Z}^{+}\mathbf{n} \\
&\approx \mathbf{u} + \mathbf{Z}^{+}\mathbf{n}
\end{aligned} \qquad (37)$$

From (32) we have

$$\mathbf{u} = \mathbf{a}s(t),$$

where

$$\mathbf{a}(r_0,z_0) = [a_1(r_0,z_0),\, a_2(r_0,z_0),\dots,\, a_M(r_0,z_0)]^T, \qquad (38)$$

$$a_m = \frac{A_m(r;r_0,z_0)}{\sqrt{k_m(r)(r - r_0)}}\, Z_m(r_0,z_0) \exp\left[-j\int_{r_0}^{r} k_m(r)dr\right], \text{ and}$$

$$s(t) = \exp(j\omega t).$$

If we define

$$\mathbf{n}' = \mathbf{Z}^{+}\mathbf{n},$$

38

(37) becomes

$$\hat{\mathbf{u}} \approx \mathbf{a}s(t) + \mathbf{n}'. \qquad (39)$$

The expression (39) is of the form (1), again for the special case of a single signal. Therefore, once $\hat{\mathbf{u}}$ is known, the MFP techniques discussed above may be used to find the emitter range and depth. As discussed earlier, no estimate of the observation noise will be used in the analysis to follow. Thus, the fact that the "noise" $\mathbf{n}'$ has a different character from $\mathbf{n}$ does not affect our analysis. The analysis for the case of the projection method is essentially the same as the foregoing and will not be presented separately. Yang [Ref. 52] notes that this method of modal decomposition gives a localization estimate which is mathematically equivalent to the MFP approach when the Bartlett processor and all modes are used.

Regardless of which method of estimating $\mathbf{u}$ is used, care is required in selecting which subset (*i.e.*, which components of $\hat{\mathbf{u}}$ and $\mathbf{a}$) of the full mode set (obtained from either (35) or (36)) is to be used, because:

- As the mode number increases, so does the vertical wavenumber [Ref. 42]; thus, for higher-order modes, a closer vertical spacing of receive hydrophones is necessary for adequate "sampling" (analogous to the sampling theorem in time-series analysis);

- Propagation models generally show greater sensitivity to uncertainties in the environmental parameters when predicting high-order modes than when predicting low-order modes (see, *e.g.*, [Ref. 52]);

- Modes which are only weakly present (*i.e.*, which have low modal amplitude) at the receiver location can generally not be estimated accurately;

- Only those modes which have most of their energy at depths within the physical extent of the receiving array are likely to be estimated accurately (see, *e.g.*, [Ref. 52]);

- When the number of receive hydrophones is less than the number of modes supported by the channel (as is the case with the data to be analyzed later in this dissertation), the inversion of (31) is an underdetermined problem and therefore cannot provide accurate values for all modes.

The first and second considerations usually favor the lower-order modes. This generalization is not valid in all situations: for example, incorporation of poorly resolved higher-order modes into the estimator can sometimes reduce sidelobe levels when the low-resolution Bartlett processor is used [Ref. 52]. The third consideration also tends to favor low-order modes, at least when the emitter and receiver are widely separated (since higher-order modes are attenuated more rapidly). The fourth consideration is relatively easy to employ, since the modal structure (*i.e.*, mode shapes) at the receiver location is known. The fifth consideration favors modes which are well sampled by the receiving array and which are therefore nearly orthogonal, since only nearly orthogonal modes are well resolved by mode filtering. Again, these modes are generally the low-order ones. In general, an initial localization estimator should be constructed based on a mode set selected using the above considerations. The peaks of this estimator may be regarded as candidate emitter locations. Then, revised estimators (one estimator per candidate

source location) may be obtained by using only those modes which are expected to be present at the receiver due to sources at these candidate locations. Thus, a strategy of iterative improvement may be used to refine the estimator.

The MMP technique may be summarized as follows:

- Perform quadrature demodulation on the received (real) signals at each receive hydrophone to obtain $\mathbf{p}(t)$;

- Use either the pseudo-inverse or projection methods to estimate $\mathbf{u}(t)$ from $\mathbf{p}(t)$ using (31);

- Generate an estimate of the modal covariance matrix $\mathbf{R}_m = E[\mathbf{u}\mathbf{u}^H]$ (or the 4th order modal cumulant matrix $\mathbf{C}_4$);

- Using a suitable propagation model and invoking the principle of acoustic reciprocity, generate the array manifold vectors $\mathbf{a}(r_0, z_0)$ (from (38)) for values of (r_0, z_0) on a suitable grid;

- Select a subset of the full mode set for use in further processing;

- Generate the functions in equations (27) (Bartlett), (28) (MVM), (29) (MUSIC), or (30) (cumulant MUSIC), as desired. The estimated emitter location is the (r_0, z_0) combination for which the function is maximized.

- As is apparent from our discussion above concerning mode selection, the major advantage (at least from the perspective of our research) of performing MFP in mode space (*i.e.*, MMP) rather than in hydrophone space is that estimation errors due to environmental

mismatch may be reduced by using by using only robust modes, which are less sensitive to such mismatch.

III. EXPERIMENTAL SETUP

This chapter provides an overview of those aspects of the Barents Sea Polar Front Experiment which are applicable to this research. This experiment provided the data on which the MFP/MMP algorithms were tested.

A. ENVIRONMENT

The data used in the analysis to follow was obtained during the 1992 Barents Sea Polar Front Experiment [Refs. 16, 17, 18, 19]. Most of the details of that experiment are not pertinent to our analysis, but may be found in the listed references; the pertinent aspects are provided below.

1. Bathymetry

Figure 7 shows the bathymetry of the acoustic channel, as well as the locations of the source (far left side of the plot) and the receiver (located at roughly 34 km range) (to be discussed later). The geometric axis from the source to the receiver was almost directly downslope.

2. Sound Speed Profile

Figure 7 and Figure 8 illustrate the sound speed field in the channel. The curves in Figure 8 were obtained by interpolation of sensor casts made at roughly 10 km intervals; the dotted and solid curves correspond to the source and receiver locations, respectively. The sound speed field obtained from the interpolation was used as input to the BBCM model for all data analysis. The higher resolution sound speed field of Figure 7 was obtained by tomographic inversion [Ref. 19]; it is provided for illustration only and was not used in our analysis.
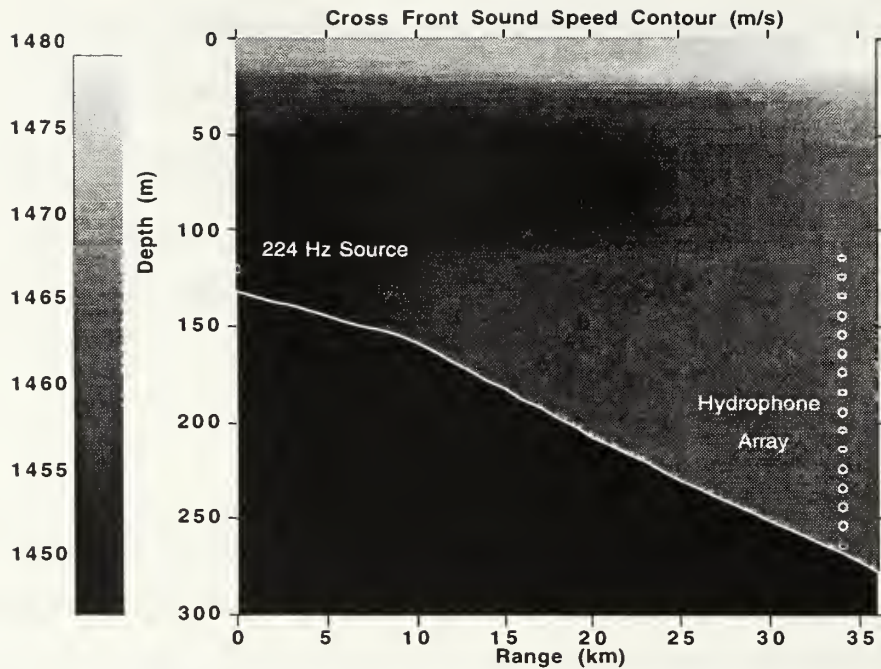
Figure 7: Sound speed field and bathymetry

The plot uses MATLAB's "pseudocolor" feature: the gray level at each point in the plot maps to a sound speed (in meters per second) per the gray level bar at the left side of the plot. The plot clearly shows the front which was the primary subject of interest in the Barents Sea Polar Front Experiment; this front was nearly perpendicular to the axis between the source and receiver. This fact, combined with the fact that sound propagation was almost entirely downslope, allows us to make the assumption that no horizontal refraction or azimuthal scattering occurred [Ref. 19]. The front was observed to move upslope and downslope with a dominant periodicity of about two hours and a peak-to-peak amplitude on the order of 4 km. The sound speed and density in the bottom were obtained from standard Navy databases and were found to be 3200 m/s and 2600 kg/m^3, respectively; these values were verified by SUS measurements [Ref. 53].
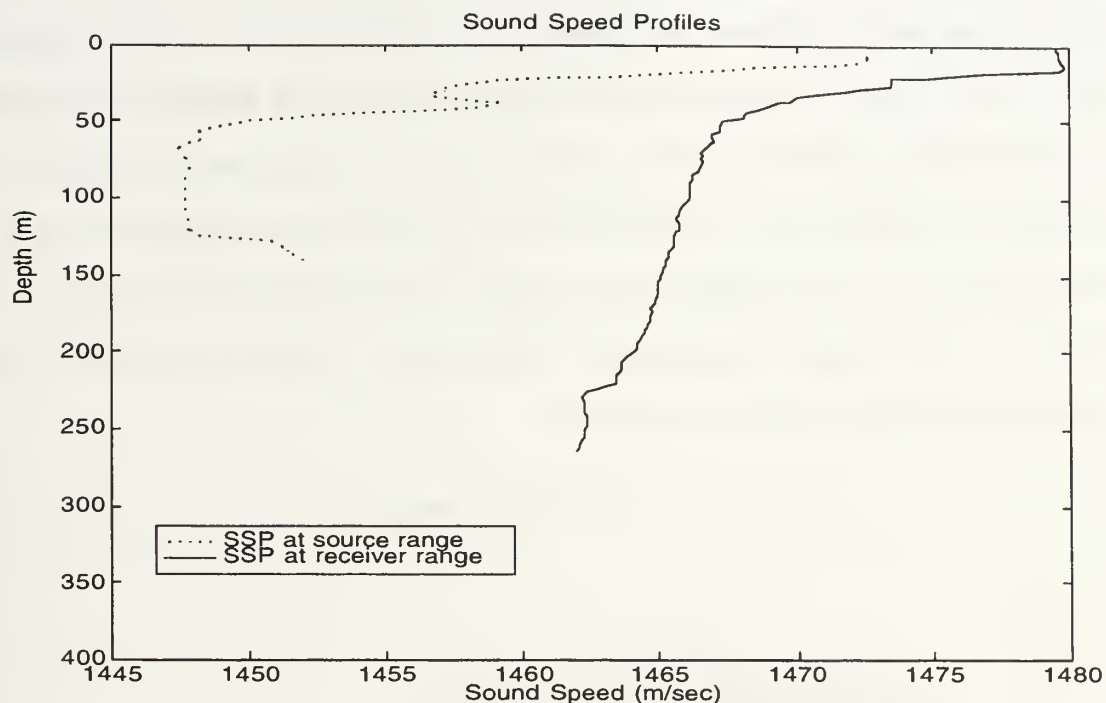
Figure 8: Sound Speed Profiles

B. SIGNAL AND NOISE

The transmitted signal consisted of M-sequences with a center frequency of 224 Hz. Two sets of M-sequences, separated by about nine hours, were transmitted during the experiment. Each set consisted of 30 M-sequences, each of about five-second duration, giving a total of about 2.5 minutes of transmission per set. The unique properties of the M-sequence were needed to achieve the goals of the Barents Sea Experiment (*i.e.*, accurate travel time determination), but are not relevant to this dissertation and will therefore not be discussed here. For the present analysis, the received signal was filtered using a Minimum-Variance filter to remove the M-sequence properties; this type of filter was selected to ensure that any strong interfering signals due to engine noise from the test ship were nulled out (see, *e.g.*, [Ref. 54]). We found, not surprisingly, that use of this filter

resulted in emitter location estimates superior to those obtained using the usual Fast Fourier Transform (FFT) approach. Figure 9 shows the power spectral density (relative to the peak) of the unfiltered received signal at a particular hydrophone and a particular time. The received signal (at 224 Hz), when averaged over all hydrophones, has a SNR of about 10 dB (ratio taken over the entire signal bandwidth); the exact value of the SNR is not particularly important for our analysis.
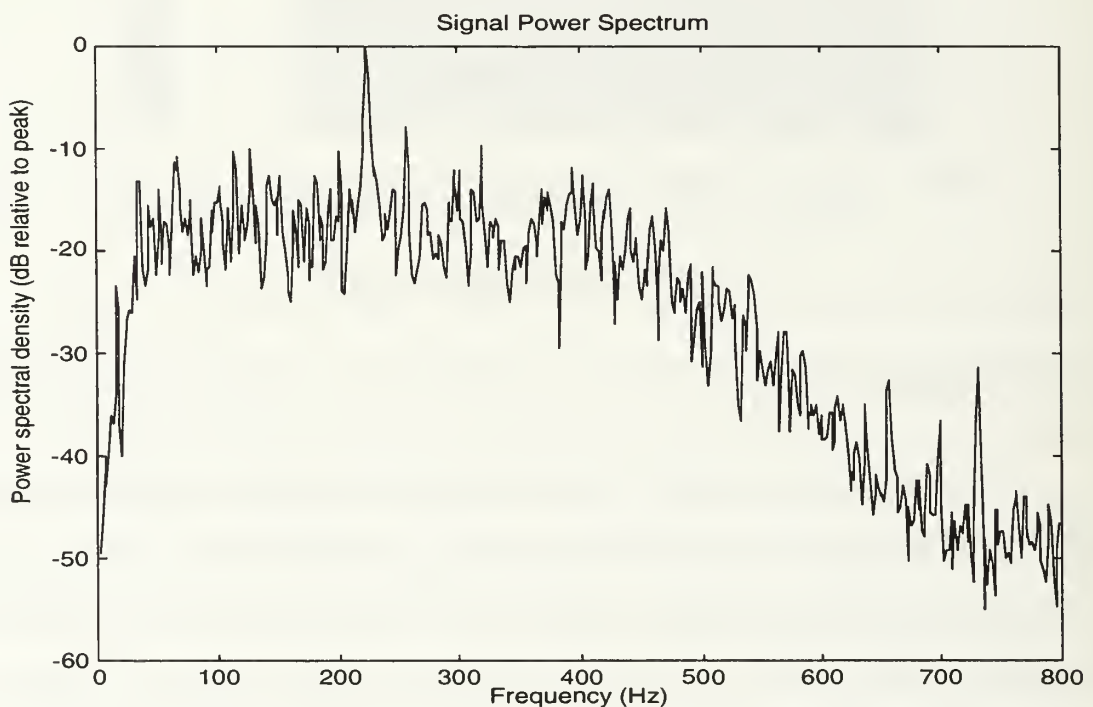
Figure 9: Power Spectrum

C. RECEIVER

The receive array consisted of a vertical string of 16 identical, omnidirectional hydrophones with 10 m spacing. The uppermost hydrophone was at a depth of 123.8 m. Prior to the collection of data used in this dissertation, hydrophones 1, 2, 4, 6–8, and 16 experienced partial failure (separation of the two piezoelectric cylinders comprising each hydrophone)

which reduced their sensitivity by 6 dB. This sensitivity reduction was incorporated into the data analysis.

IV. ANALYSIS AND RESULTS

This chapter provides further details of the analytical technique, including preprocessing methods. It also provides and interprets our main results (which take the form of ambiguity surface plots) from application of the MFP/MMP estimators to the Barents Sea data for various choices of parameters (noise, data length, etc.).

A. ANALYSIS TECHNIQUE

1. Signal Processing

The computational procedure may be outlined as follows:

- Construct the density and sound speed fields (functions of range and depth) from *in situ* measurements using bilinear interpolation);

- Using sound speed, density, receiver horizontal location, and bathymetry as inputs, and regarding each receive hydrophone as a unit emitter, generate (using a suitable propagation model) and store the parameters appearing in (31) (a separate set of parameters for each hydrophone depth);

- Using a numerical implementation of (31) and invoking the principle of acoustic reciprocity, calculate the array manifold on a suitable grid of (r_0, z_0) values;

- Take the raw hydrophone data (an M-sequence) and add the desired amount of noise (measured in the same environment during a period when no transmissions occurred);

- Pass the resulting signal through a 50th order minimum-variance filter to eliminate out-of-band noise and to remove the M-sequence properties from the signal (*i.e.* make it into an ordinary narrow-band process);

- Calculate estimated spatial and modal covariance and cumulant matrices from the resulting signal;

- Match these covariance matrices against the replica fields calculated above (for MMP, use only the components corresponding to the desired modes).

All computations were done using Matlab 4.2c on a Hewlett-Packard 735 Workstation. The propagation modeling used the Broadband Coupled Mode (BBCM) algorithm [Ref. 19]. In every case, the ambiguity surfaces were calculated for a grid with the following specifications, selected to ensure peaks would not be missed while keeping the computational load reasonable:

Parameter	Minimum	Maximum	Increment
(Emitter) Range	15 km	40 km	40 m
Depth	2 m	146 m	2 m

Table 1: Computation grid

The emitter range used in the plots is measured with respect to a reference different from those shown in Figure 6 and Figure 7: it is measured with respect to a point 1675 m downslope from the receiver. The 15–40 km range window was selected to allow a fair assessment of our estimators, while keeping the amount of computation manageable. Because the water gets deeper as one gets closer to the receiver, more modes are required to construct the pressure field (the number of modes supported is roughly proportional to the water depth for a fixed frequency). The run time required

by the BBCM model appears to be proportional to the number of modes cubed.

2. Plotting

The ambiguity surface plots were generated using Matlab (version 4.2a) on a Macintosh LCIII and printed on a 600 dot per inch (dpi) HP LaserJet 4, using the Matlab "pseudocolor" plot function with 32 gray levels. Because a 600 dpi printer is not able to generate a dot screen with adequate resolution to display data on a grid as large as that found in Table 1 without requiring an excessive amount of space on the page, the ambiguity surface data was smoothed before plotting: at each depth grid point, the value plotted is the average for three adjacent range grid points. Subjectively speaking, little information appeared to be lost as a result of this smoothing.

The quantitative assessment of the effect of various parameters on localization performance presents an interesting problem. On all plots, the bright areas correspond to maxima of the functions (27) through (30). No gray scale is provided, since, for the MUSIC algorithm, the peak height does not necessarily correspond to the power of the received signal. In fact, the values corresponding to "white" and "black" differ somewhat from plot to plot. A more suitable approach for quantitatively comparing the different plots may be based on three major performance measures used in DOA estimation literature (see, *e.g.*, [Ref. 23]):

- Bias in the emitter location estimates;

- Ability to resolve multiple closely spaced emitters; and

- Existence of peaks at locations where no emitters exist.

In the present case, because the *precise* location of the emitter is not known, the first measure is not applicable in the form stated. Also, only one emitter is present, so the second measure is not particularly useful either. The third measure is applicable, although not easy to quantify. We have elected instead to use the following:

- Ratio of the height of the correct peak to that of the highest false peak (M1);

- Size (area) of the correct peak relative to the area of the entire grid (M2);

- Ratio of the average height of all false peaks to the height of the correct peak (M3).

Obviously, when M1<1, an incorrect estimate for the emitter location will be obtained. The values of these three measures are given in the caption for each figure that follows.

B. OVERVIEW OF RESULTS

In each section to follow, we consider the effect of the variation of a single parameter (*e.g.*, data length, algorithm type, SNR, etc.) while holding all other parameters fixed at the following nominal values (for which performance is good):

- Matched-mode method (using projection method of mode filtering and modes 1–4);

- Data length of 1024 points;

- Data taken from the beginning of the second set of M-sequence transmissions;

- SNR=10 dB (*i.e.*, no noise beyond that actually observed with the signal);

- MUSIC method of array processing;

- Second-order statistics;

- Coupled-mode propagation model; and

- Hydrophone data corrected for reduced sensitivity of damaged phones.

Each plot to follow has a title at the top containing the most significant parameters (MFP/MMP, SNR, data length, and array processing algorithm). Additional pertinent information appears either in the caption or in the text referring to the plot. In every case, the correct emitter location is at approximately 36 km range and 122 m depth.

C. MATCHED-FIELD VERSUS MATCHED-MODE PROCESSING

As mentioned earlier, propagation models are generally more sensitive to errors in knowledge of the environment when predicting high-order modes than low-order modes. We therefore expect MFP to exhibit a higher incidence of false peaks than MMP, since MFP uses all available modes (26). Figure 10 (MFP) and Figure 11 (MMP) illustrate this effect. For purposes of illustration, we have added a small white circle at the correct emitter location in Figure 10, although we have not done so with subsequent plots, because the emitter location is fixed. Although MFP gives a peak at approximately

the correct emitter location (M1=0.94), there are 2 other peaks which are higher, as well as numerous smaller peaks (M3=0.043). MMP gives the highest peak at the correct location (M1=1.7) and has fewer and smaller false peaks (M3=0.016).
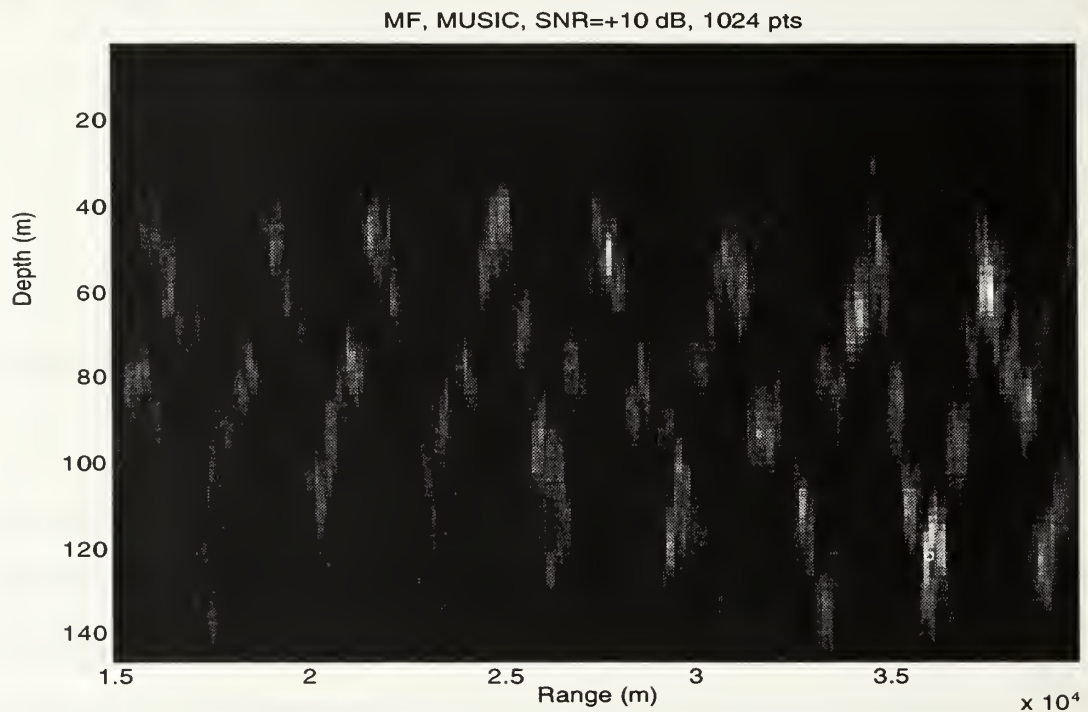
Figure 10: Matched-Field Processing (M1=0.94; M2=0.0077; M3=0.043)
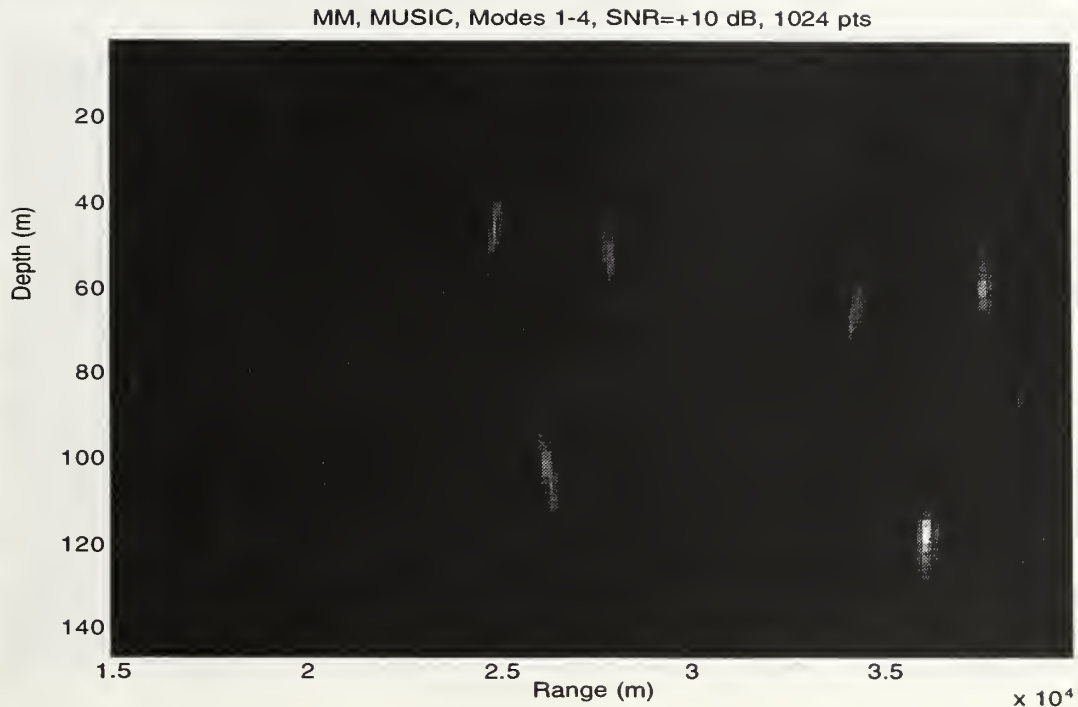
Figure 11: Matched-Mode Processing (M1=1.7; M2=0.012; M3=0.016)

D. BEHAVIOR OF DIFFERENT ARRAY PROCESSING METHODS

Both Figure 12 (MVM) and Figure 13 (Bartlett) show poor resolution compared with MUSIC (Figure 11). Both of these methods produce the largest peak at the correct location (M1=1.26 and 1.03, respectively), but there are large and numerous false peaks (M3=0.11 and 0.14, respectively). In particular, with the Bartlett method, the correct peak is nearly impossible to identify visually. The behavior of these three methods when used on this data set is thus consistent with that observed in DOA estimation and with modeled MFP data (see, *e.g.*, [Refs. 3, 23]).

MM, MVM, Modes 1-4, SNR=+10 dB, 1024 pts
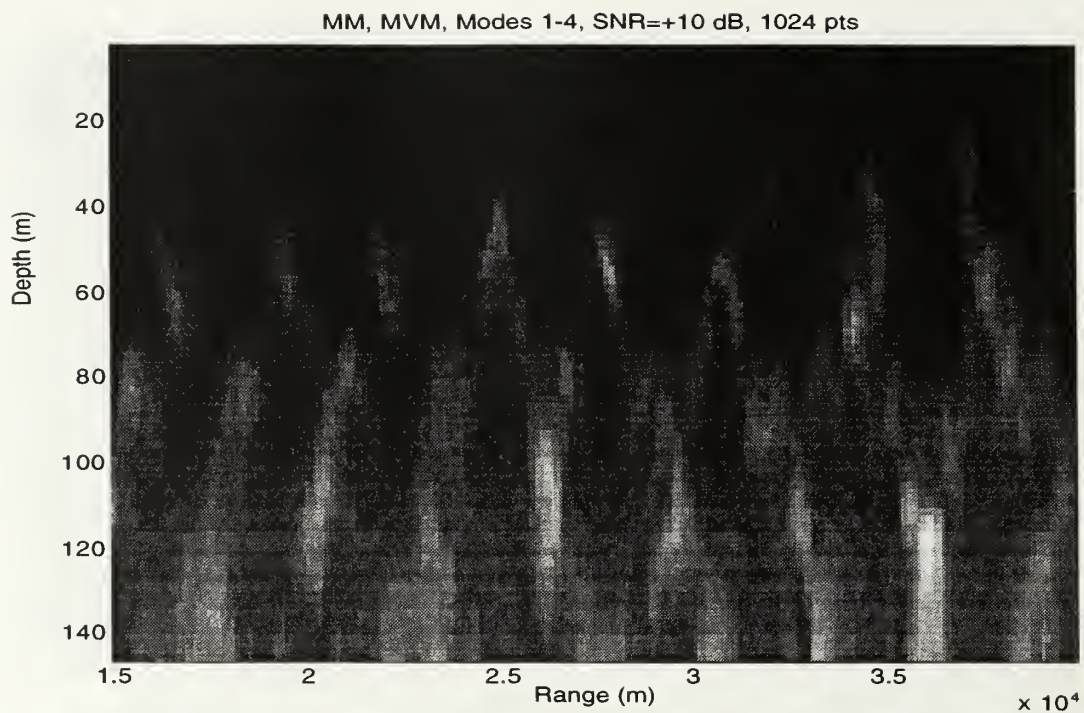
Figure 12: Minimum-Variance Method (M1=1.26; M2=0.033; M3=0.11)

MM, Bartlett, Modes 1-4, SNR=+10 dB, 1024 pts
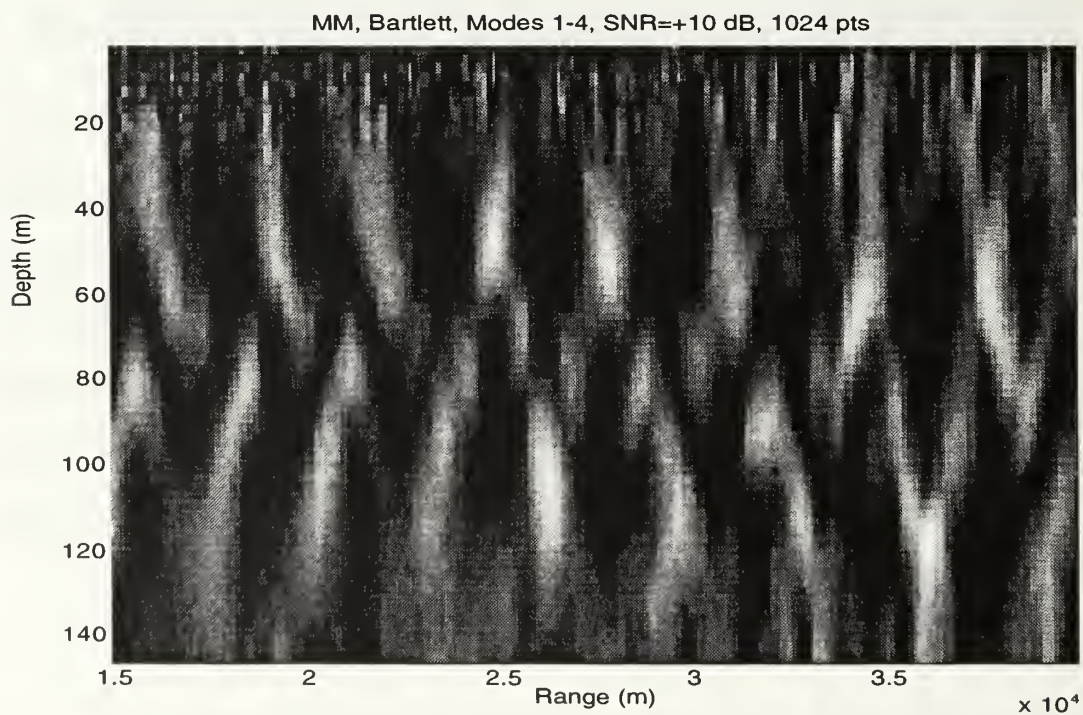
Figure 13: Bartlett Method (M1=1.03; M2=0.017; M3=0.14)

E. EFFECT OF DATA LENGTH ON PERFORMANCE

As the length of data increases (assuming temporally stationary data and fixed SNR), the accuracy of the estimate of spatial covariance should improve. On the other hand, if significant non-stationarity is present, we expect that increases in data length past a certain point (depending on SNR) may actually degrade the accuracy of this estimate. This is the case with our data, as may be seen in Figure 14 through Figure 16, where the ambiguity surface for a data length of 512 shows some improvement (M1=2.2, M3=0.015) with respect to the surface for a data length of 1024 (Figure 11), and the size of the false peaks increases noticeably for data lengths of 2048 (M1=1.6, M3=0.019) and 4096 (M1=1.4, M3=.020). This behavior is presumably due to surface wave effects, which are the only likely source of temporal variability over the roughly one-second time scale involved here. Obviously, data length can only be reduced so far before the benefits gained by avoiding non-stationarity are outweighed by estimation errors arising from low information-to-noise ratio. In fact, performance degradation became evident at SNR=+10 dB when the data length was reduced to 256 points (not shown).

MM, MUSIC, Modes 1-4, SNR=+10 dB, 512 pts
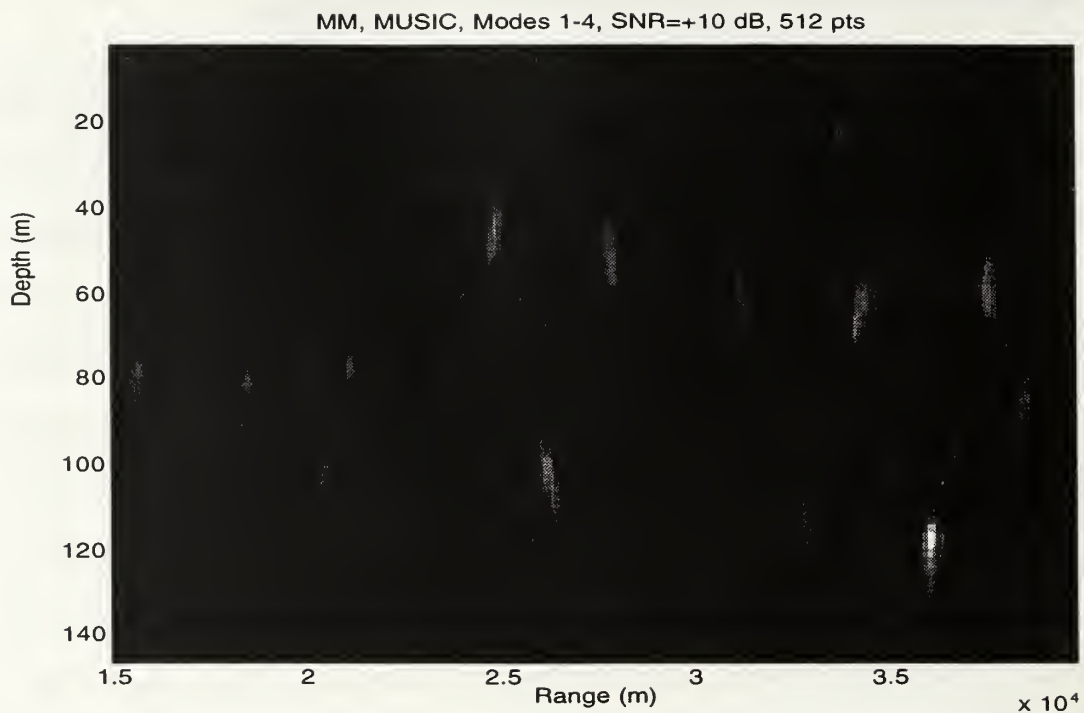
Figure 14: Data Length 512 (M1=2.2; M2=0.012; M3=0.015)

MM, MUSIC, Modes 1-4, SNR=+10 dB, 2048 pts
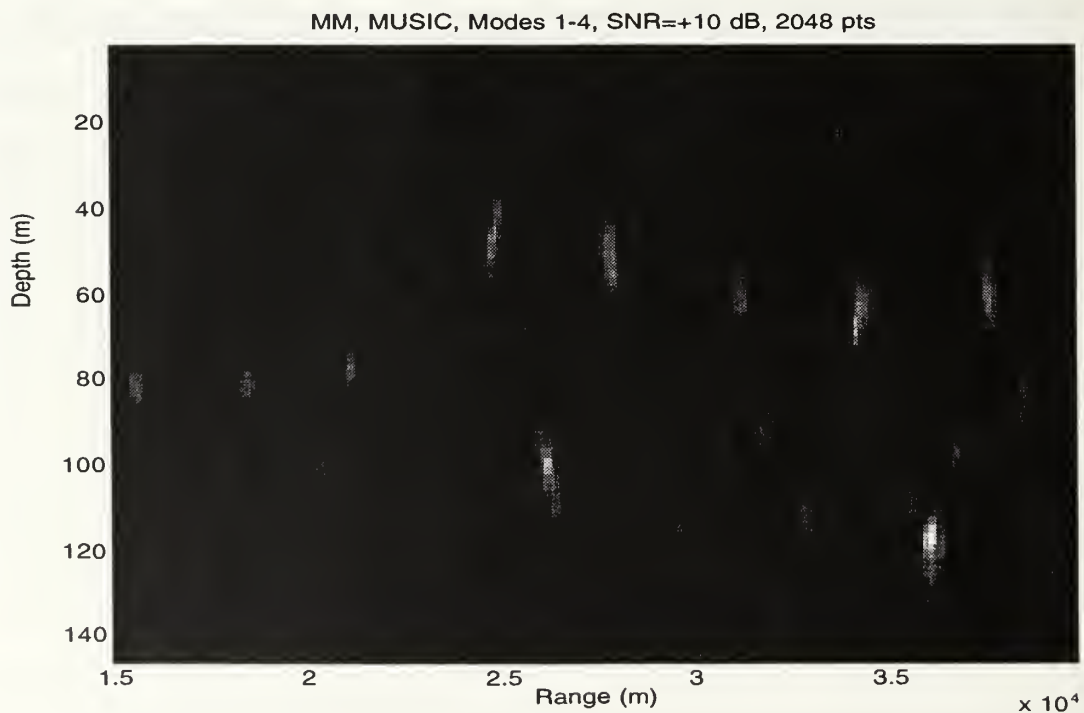
Figure 15: Data Length 2048 (M1=1.6; M2=0.012; M3=0.019)
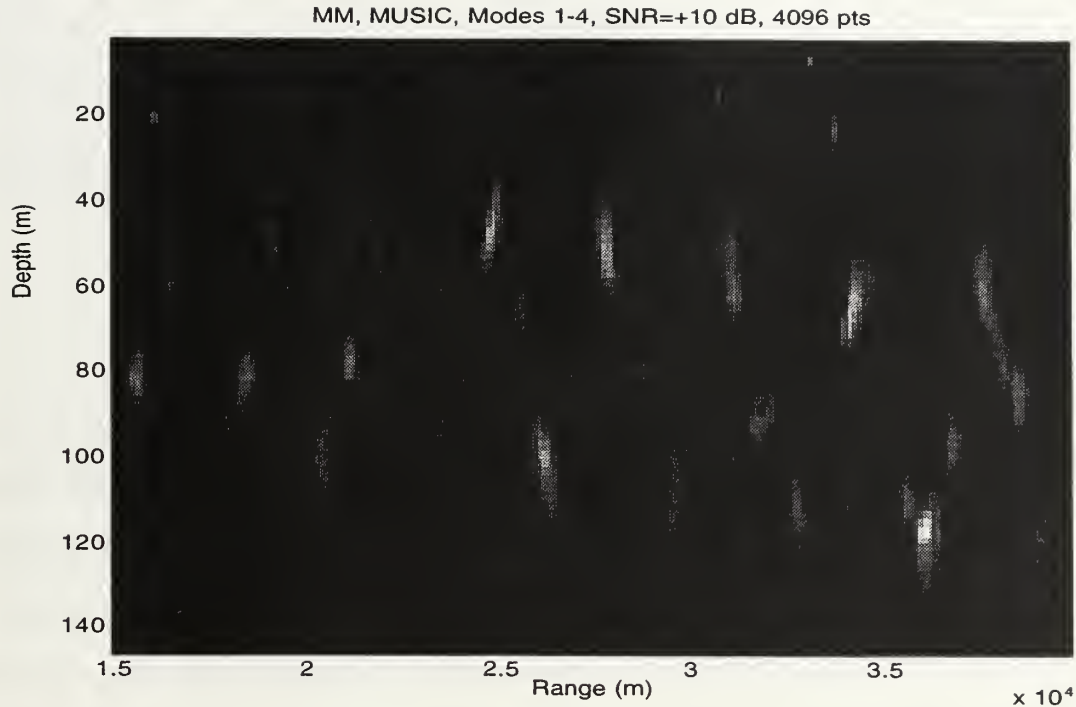
Figure 16: Data Length 4096 (M1=1.4; M2=0.012; M3=0.020)

F. EFFECT OF NOISE ON PERFORMANCE

Figure 17 through Figure 19 illustrate the effect of additive noise. These plots exhibit high false peaks compared with Figure 11 (no added noise). Below a SNR of –10 dB, the MUSIC method using 2nd order statistics no longer gives the largest peak at the actual emitter location (M1=0.72 for Figure 18). Interestingly, the MUSIC method with 4th-order statistics actually gives poorer results than with 2nd-order statistics at all SNRs (Figure 19 shows the 0 dB result). One reason for this somewhat surprising result appears to be that the signal turns out to be roughly as close to Gaussian as the additive noise, as measured by the difference between its 4th-order moment and the 4th-order moment of a Gaussian process with the same lower-order moments (11). Specifically, let us define a measure G for quantifying Gaussianity for the received signal as follows:

59

$$G = \frac{\|\mathbf{C}_4\|_F}{\|\mathbf{M}_4\|_F}, \tag{40}$$

where $\|\cdot\|_F$ indicates the Frobenius norm*, $\mathbf{C}_4$ is defined by (14), and $\mathbf{M}_4$ is the matrix of 4th order moments; *i.e.*,

$$\mathbf{M}_4(i, j) = E\left[p_i p_i^* p_j p_j^*\right].$$

As discussed earlier, if the processes p_i are Gaussian, $\mathbf{C}_4=0$ and therefore $G=0$. We find that, in this experiment, for noise alone, $G=0.13$ and for signal alone $G=0.12$ (the use of different norms in (40) does not significantly affect these values). Recall that our motivation for using higher-order statistics in the first place was based on an expectation that the noise would be Gaussian and the signal would not. It appears that this Gaussian property is characteristic of the filtered M-sequence signal; for continuous wave (CW) data gathered later in the experiment (at which time, unfortunately, environmental measurements are not available), G is significantly higher.

---

* The Frobenius norm of a matrix $\mathbf{A}$ is defined as $\|\mathbf{A}\|_F = \sqrt{\sum_{i,j} |A_{ij}|^2}$, where A_{ij} are the components of $\mathbf{A}$.

MM, MUSIC, Modes 1-4, SNR=-10 dB, 1024 pts
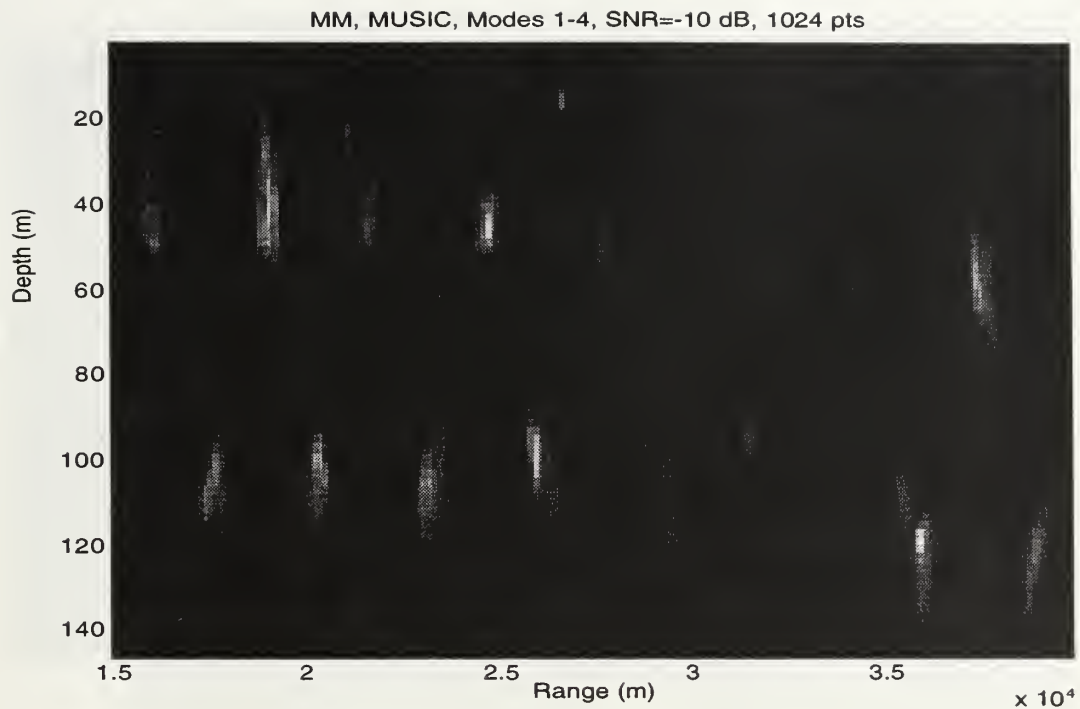
Figure 17: SNR = –10 dB, 2nd order statistics
(M1=1.1; M2=0.014; M3=0.028)

MM, MUSIC, Modes 1-4, SNR=-11 dB, 1024 pts
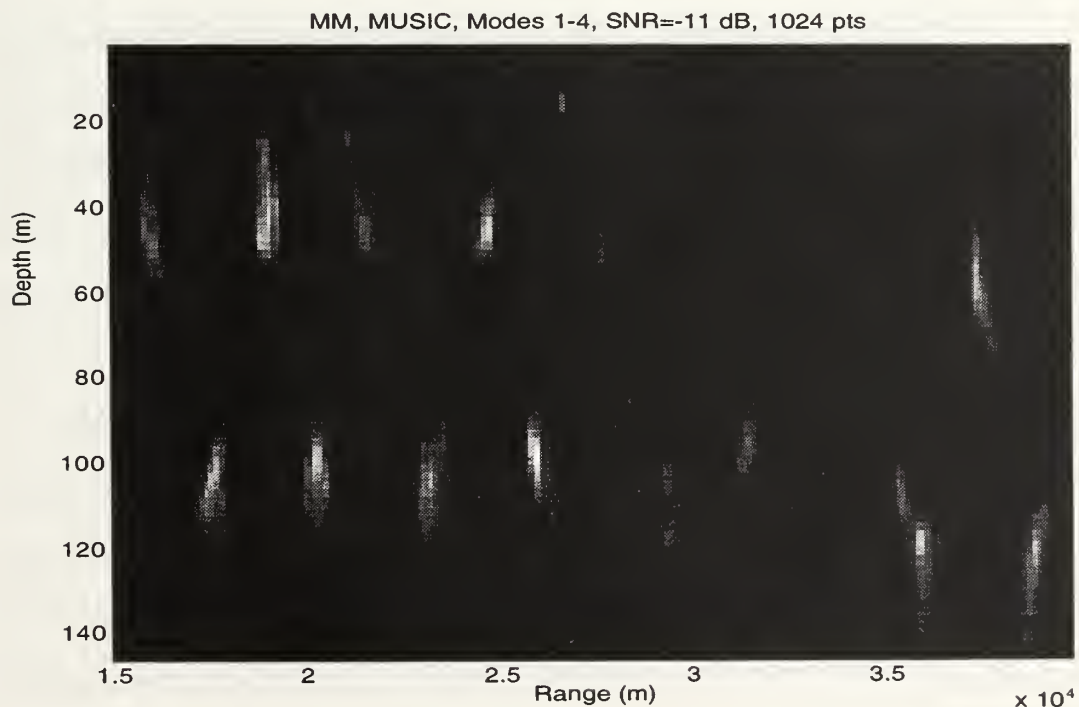
Figure 18: SNR = –11 dB, 2nd order statistics
(M1=0.72; M2=0.012; M3=0.035)

61
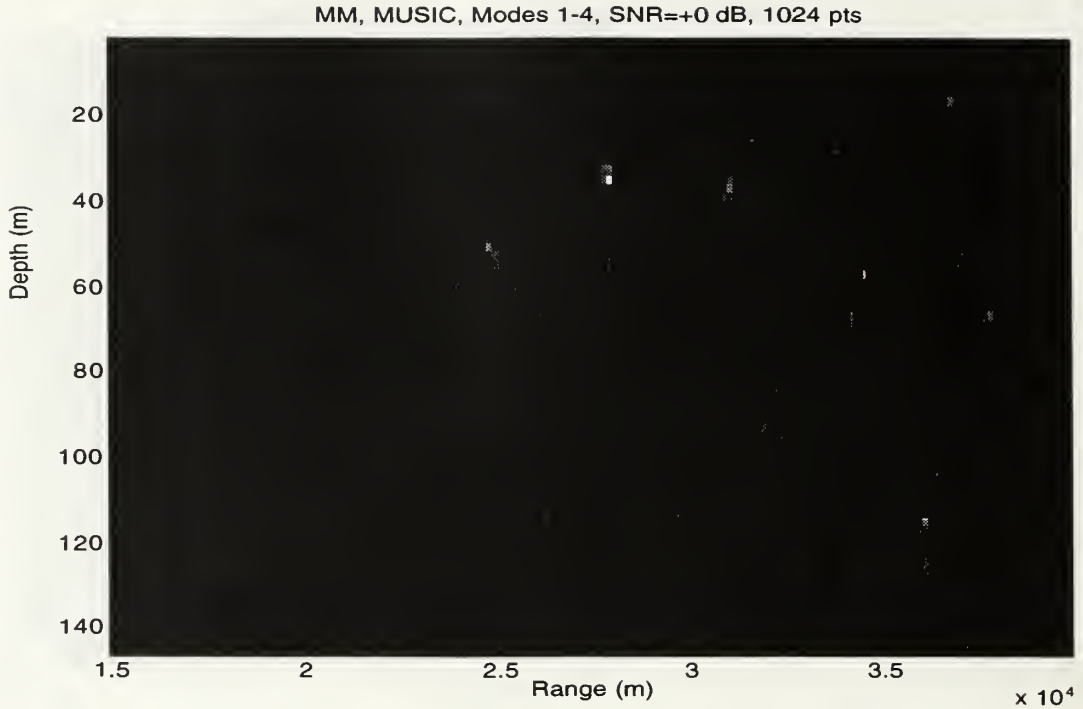
Figure 19: SNR = 0 dB, 4th order statistics
(M1=0.34; M2=0.008; M3=0.015)

A more significant flaw in the cumulant-based MUSIC estimator is illustrated in Figure 20 through Figure 23, which show the performance of cumulant-based MUSIC MFP versus that of conventional MUSIC MFP when applied to a *synthetic* data set (no mismatch between the actual and predicted sound fields) for SNRs of +10 dB and 0 dB. At +10 dB, the cumulant-based method (M1=12.3) greatly outperforms the conventional method (M1=2.9). However, at 0 dB, the conventional method is superior (M1=2.7 vs. M1=1.6), despite the fact that the signal subspace is estimated much more accurately for the cumulant method than for the conventional method (as quantified by the angle between the signal subspaces at +10 dB and 0 dB). This behavior is due to the fact that both the cumulant matrix $\mathbf{C}_4$ and the array manifold vectors ($\mathbf{a} \circ \mathbf{a}^*$) are defined to be real: since both MFP and MMP rely heavily on phase information for accurate localization, use of amplitude information

alone causes the estimators to be highly sensitive to noise-induced errors in the estimate of C_4.
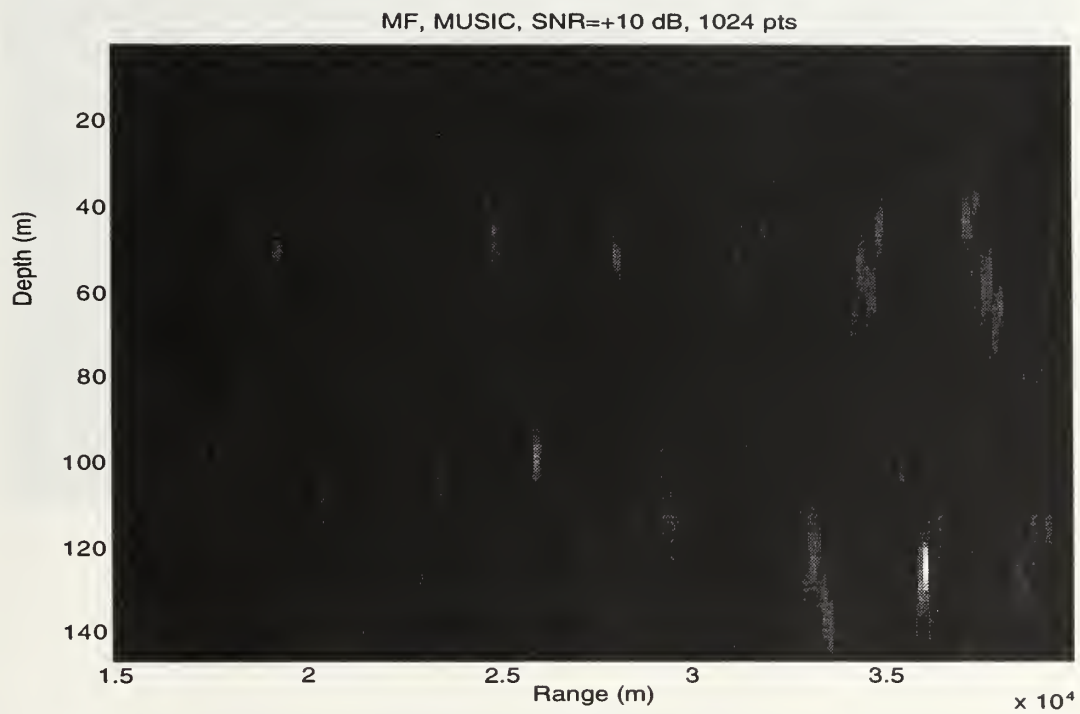
**Figure 20: Conventional MUSIC, synthetic data
(M1=2.9, M2=0.0091, M3=0.014)**

MF, MUSIC, SNR=+10 dB, 1024 pts
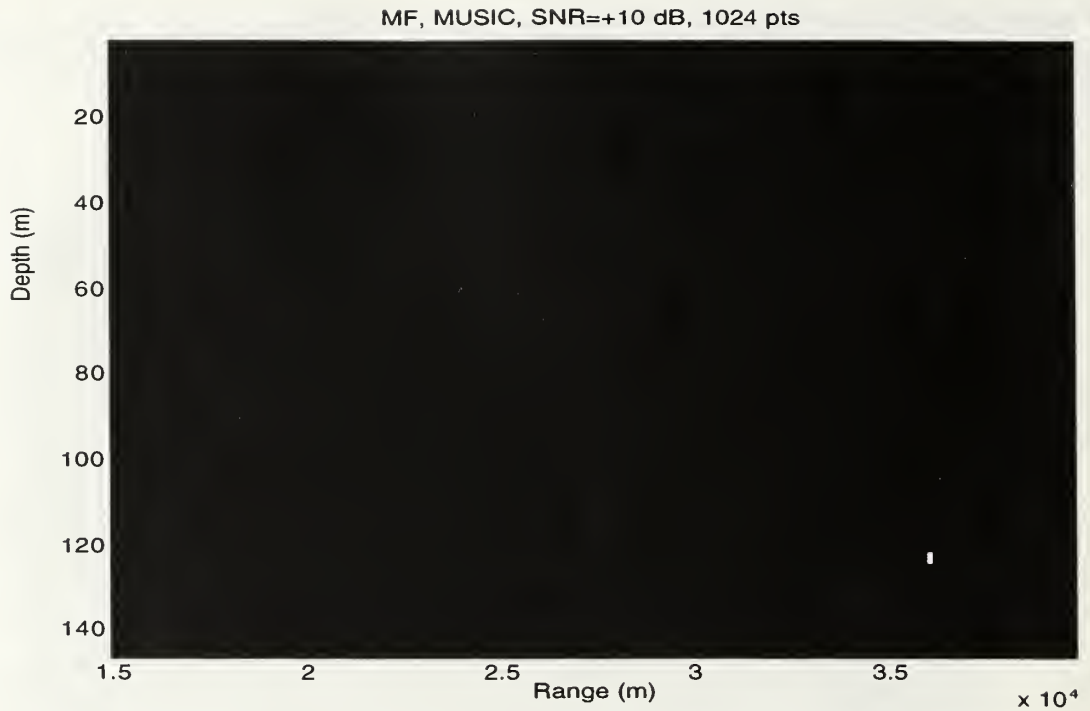
**Figure 21: Cumulant MUSIC, synthetic data
(M1=12.3, M2=0.0021, M3=0.0022)**

MF, MUSIC, SNR=+0 dB, 1024 pts
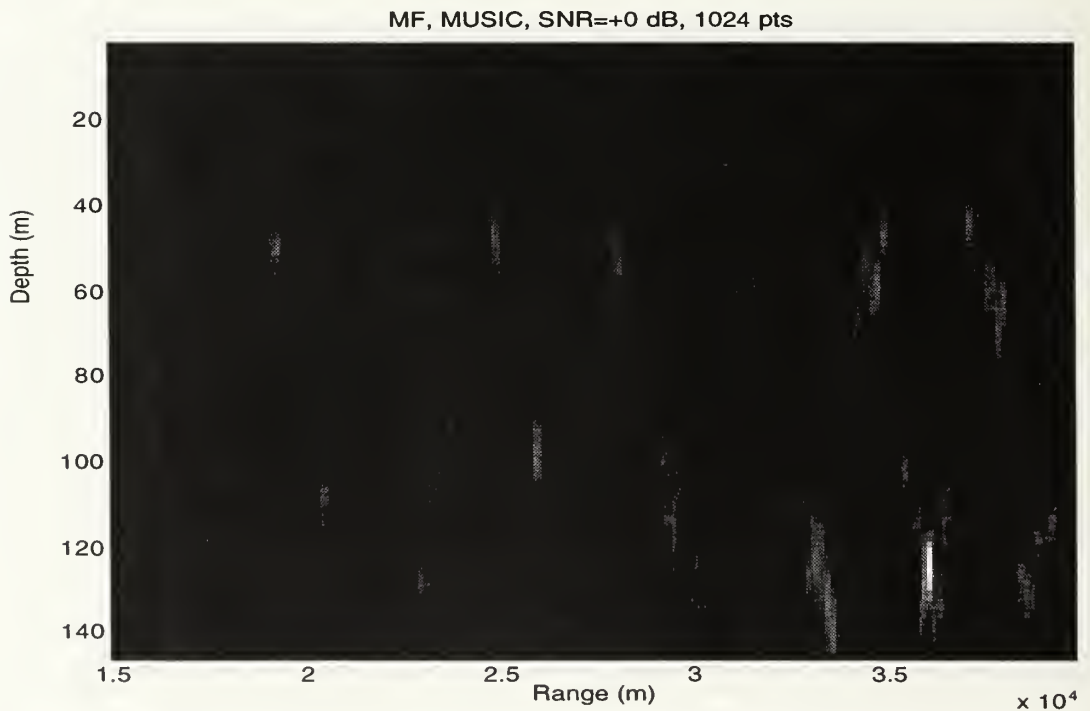
**Figure 22: Conventional MUSIC, synthetic data
(M1=2.7, M2=0.0093, M3=0.015)**

64

MF, MUSIC, SNR=+0 dB, 1024 pts
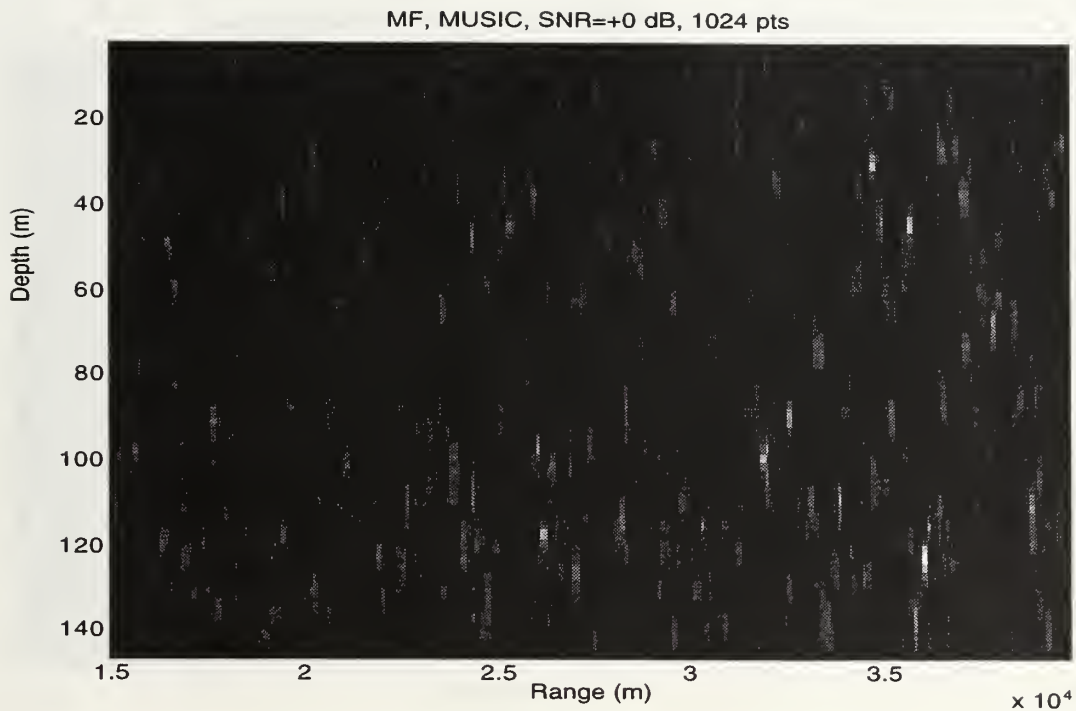
**Figure 23: Cumulant MUSIC, synthetic data
(M1=1.6, M2=0.0022, M3=0.015)**

G. BEHAVIOR OF DIFFERENT MODE INVERSION METHODS

Figure 24 shows the result when the pseudoinverse method is used instead of the projection method. As mentioned above, the two methods are very similar mathematically and give about the same performance (compare with Figure 11). The false peaks are slightly larger and more numerous with the pseudoinverse method (M3=0.020 vs. 0.016 for the projection method).
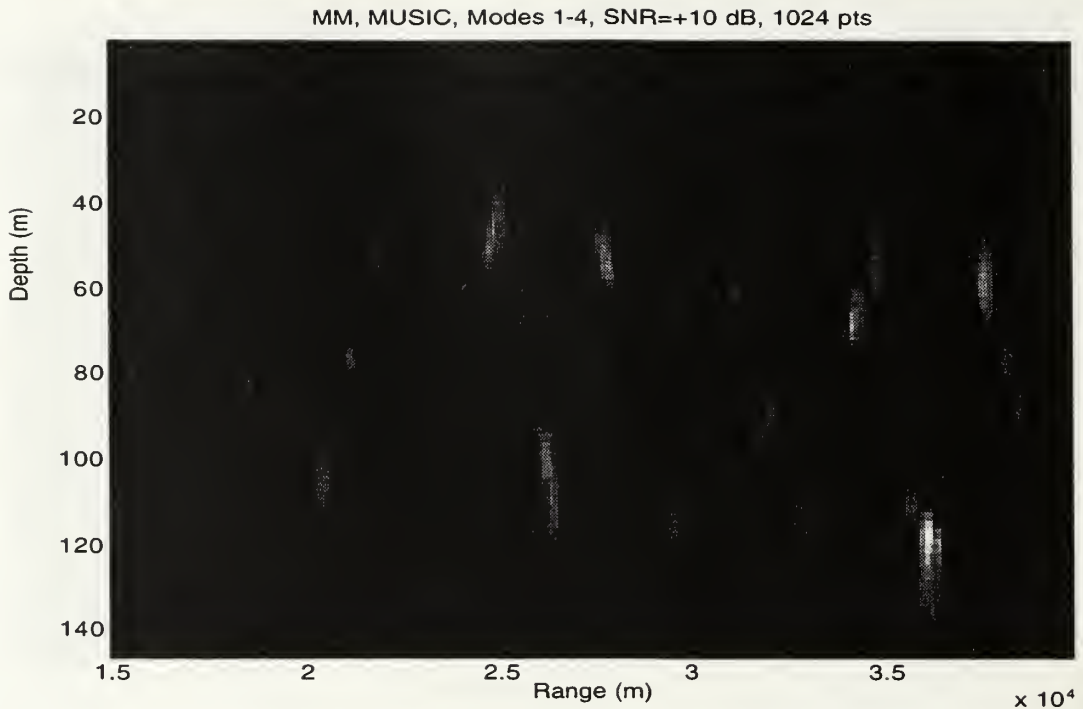
Figure 24: Pseudo-inverse mode filter (M1=1.7; M2=0.013; M3=0.020)

H. EFFECT OF ARRAY SHADING

Figure 25 shows the effect of not including the required sensitivity correction for the failed hydrophones (*i.e.,* no array shading). The higher false peaks are apparent (M1=1.1 and M3=0.025, as compared with M1=1.7 and M3=0.016 when shading is used).

66

MM, MUSIC, Modes 1-4, SNR=+10 dB, 1024 pts
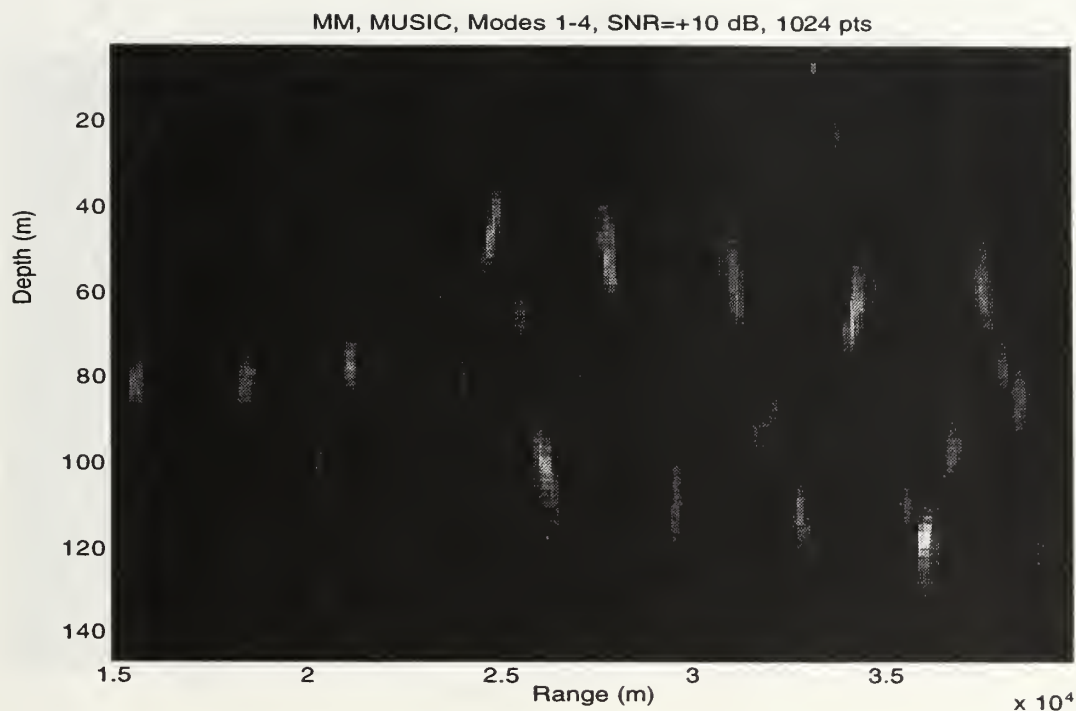
**Figure 25: No phone sensitivity correction
(M1=1.1; M2=0.012; M3=0.025)**

I. TEMPORAL VARIABILITY OF RESULTS

Figure 26 shows the results from a data segment obtained during the first set of M-sequence transmissions. Although there is a peak at the correct emitter location, it is not the largest peak (M1=0.46). The change in localization performance with respect to that obtained with a data segment from the second set of transmissions is probably due to temporal fluctuations in the sound speed field, since none of the other physical parameters changed significantly between the two data sets. This behavior is not surprising, since the period of frontal motion (two hours) is much less than the time between the sets of M-sequence transmissions. Although the plots are not shown here, we found that the localization performance remained qualitatively the same for all data segments within a given set of transmissions.
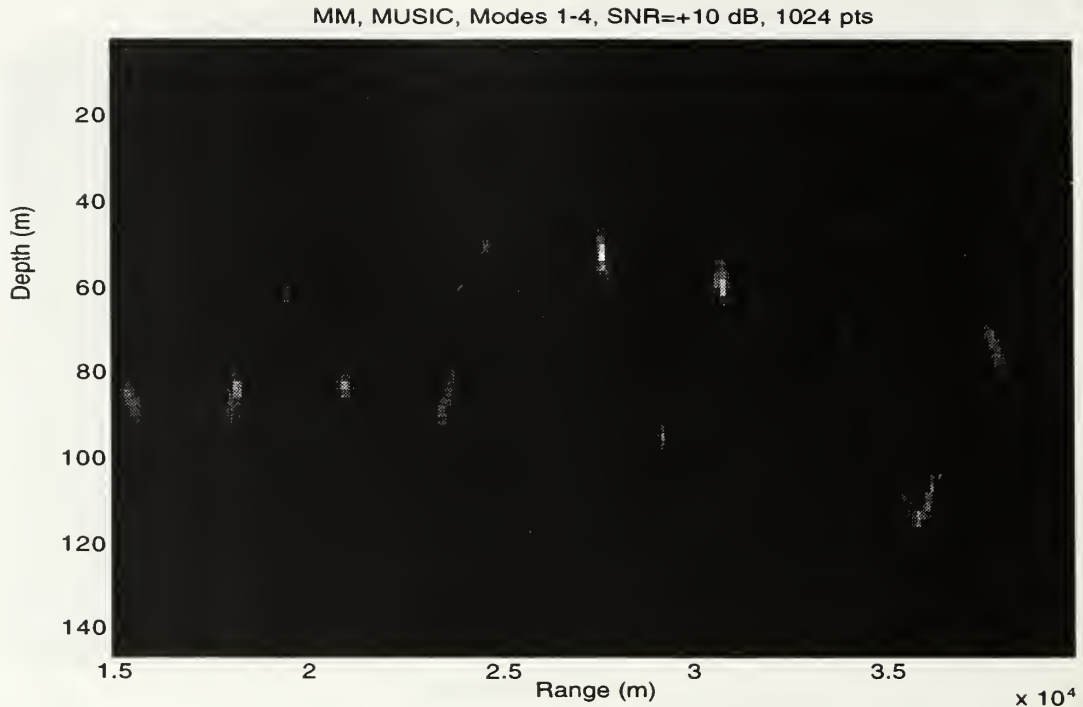
Figure 26: Data from 1st transmission (M1=0.46; M2=0.015; M3=0.026)

J. EFFECT OF MODE SELECTION ON MMP RESULTS

As discussed above, it is important to choose a suitable mode subset to ensure satisfactory results. Obviously, with 60 modes available, there is a very large number of potential combinations, only a few of which will be presented here. Figure 27 shows the result when only the first 3 modes are used; a small peak is visible at the correct location (M1=0.46). Figure 28 shows the result when modes 1–5 are used; the plot shows a slight improvement in performance compared to the result with modes 1–4 (M1=1.8 and M3=0.015 vs. 1.7 and 0.016, respectively). Using more than the first five modes tends to increase the number and size of the false peaks. Figure 29 (modes 1–6 used) shows this effect (M1=1.3, M3=0.018).

MM, MUSIC, Modes 1-3, SNR=+10 dB, 1024 pts
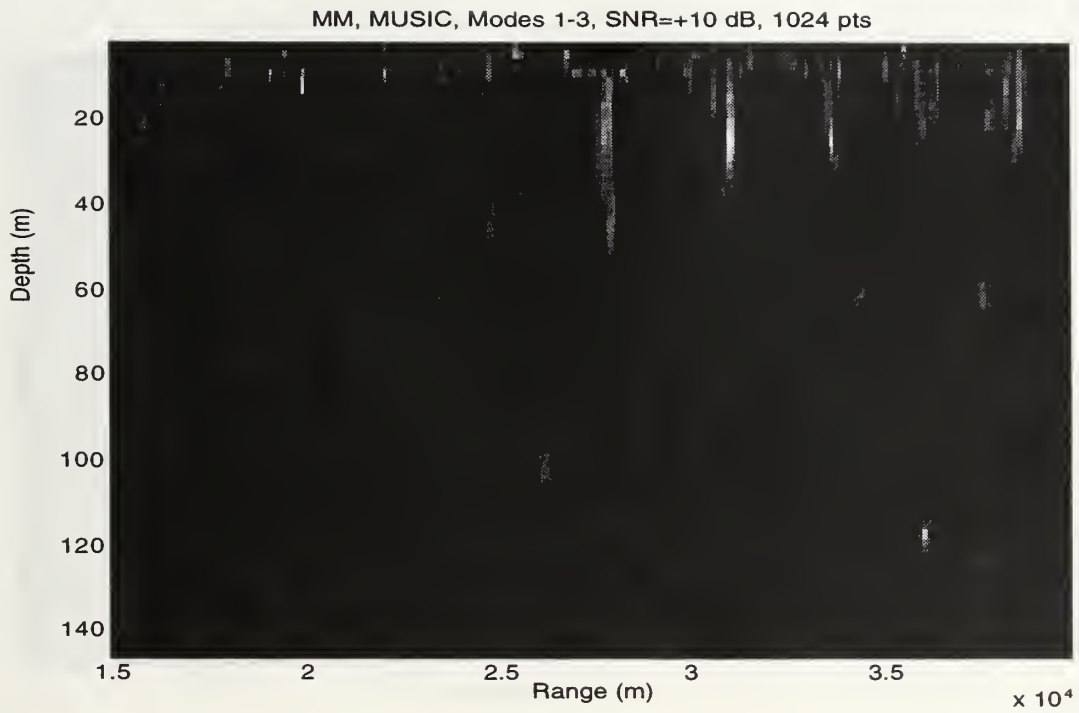
Figure 27: Modes 1–3 (M1=0.46; M2=0.0070; M3=0.025)

MM, MUSIC, Modes 1-5, SNR=+10 dB, 1024 pts
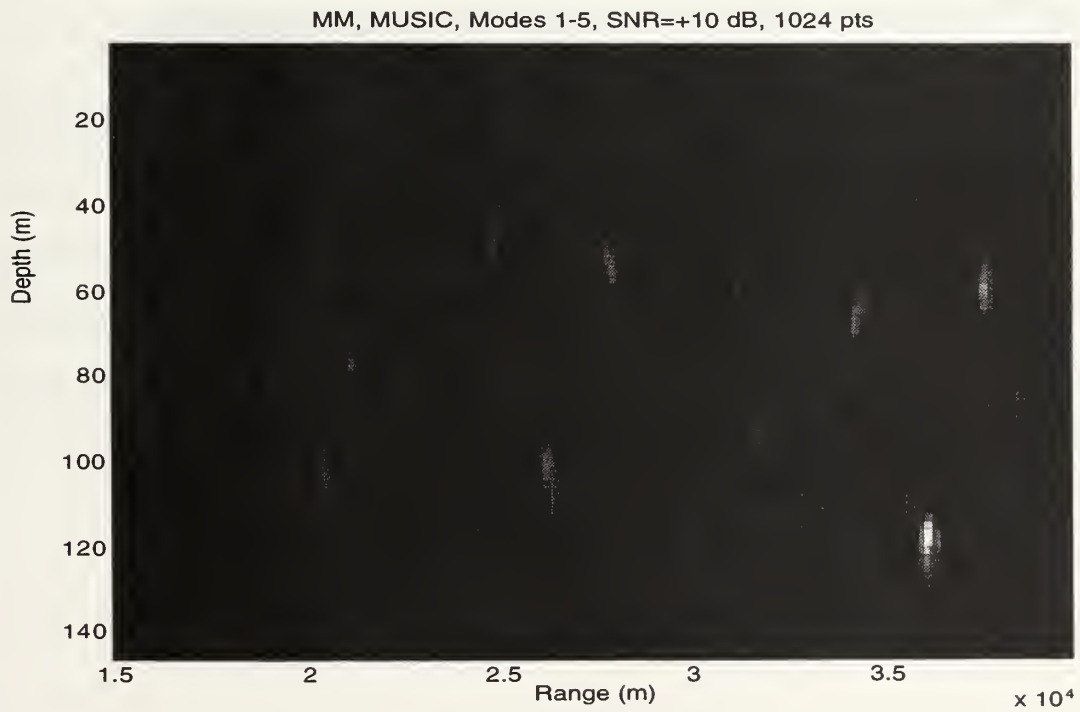
Figure 28: Modes 1–5 (M1=1.8; M2=0.011; M3=0.015)
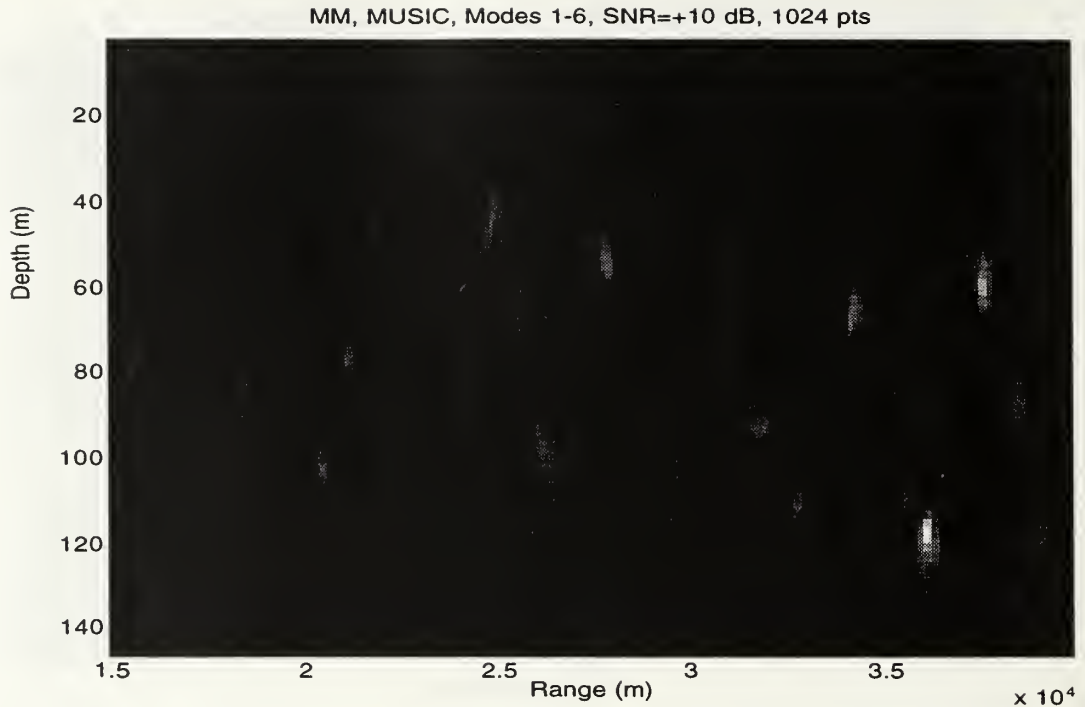
69

MM, MUSIC, Modes 1-6, SNR=+10 dB, 1024 pts

Figure 29: Modes 1–6 (M1=1.3; M2=0.011; M3=0.018)

K. EFFECT OF MODEL SELECTION ON PERFORMANCE

Figure 30 shows the result when the mode coupling accounted for by the BBCM method is not included in calculation of the replica fields, that is, when the range dependence of the replica fields arises only from the range dependence of the mode functions and wavenumbers (the adiabatic approximation of (22)). There is no indication of a peak at or near the actual emitter location, so the performance measures M1, M2, M3 are meaningless and are not provided.

MM, MUSIC, Modes 1-4, SNR=+10 dB, 1024 pts
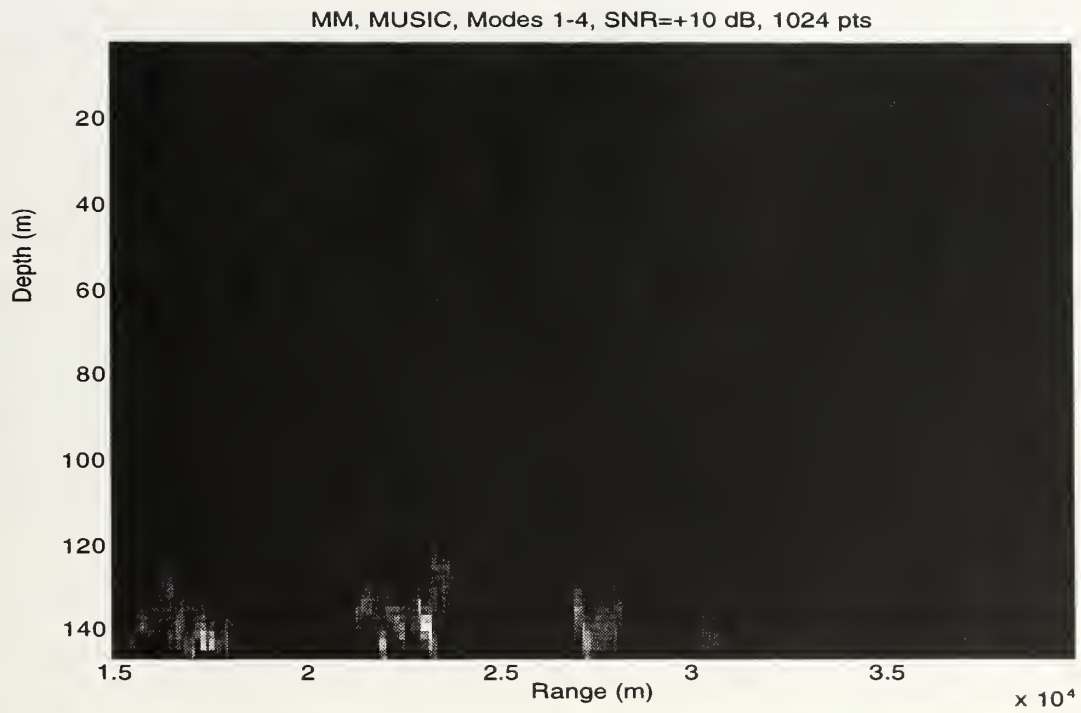
Figure 30: Adiabatic model

V. CONCLUSIONS

The results presented in the body of this dissertation clearly demonstrate that MUSIC-based MMP techniques may be effectively employed even in a very challenging acoustic environment such as that which existed during the Barents Sea Polar Front Experiment. It is appropriate to review some of the unique features of this environment (as compared to idealized numerical simulations or simple experiments):

- Strong range dependence of bathymetry and the sound speed field (which included a strong, rapidly moving front);

- A degraded receive array spanning about half the water column and having many fewer elements than the number of modes supported by the channel;

- Relatively coarse sampling of the sound speed field (only about once per 10 km interval, notwithstanding the presence of a front);

Despite these challenges, we achieved considerable success with our localization approach. Some of the specific findings and original contributions of this research are:

- Contrary to much conventional wisdom, the subspace-based MUSIC method produced good results despite the inaccuracies inherent in experimental data. In fact, the MUSIC algorithm's high resolution was vital to accurate localization, because the receive array was relatively short and few robust modes were available.

73

- The Broad Band Coupled Mode (BBCM) model generates replica fields with sufficient accuracy to allow localization via MMP in this strongly range-dependent environment. The adiabatic approximation was found to be grossly inadequate for this environment.

- The cumulant-based MUSIC estimator used in this dissertation was too sensitive to noise-induced and model-induced estimation errors to be useful with real data. This behavior was due to the fact that the cumulant matrix and the replica fields were defined as real quantities; thus, the phase information, which is vital to robust and accurate localization, was not available.

- In an environment with strong temporal variability, localization performance can vary drastically over relatively short time scales.

In summary, our approach, which combined the high-resolution MUSIC algorithm with MMP, allowed accurate localization estimates, even though only a few robust modes could be obtained via mode filtering.

The approach used in our analysis may be modified in three obvious respects, each of which offers potentially significant improvement in localization performance and is worthy of further study.

The first modification relates to the assumptions concerning observation noise. The basic MUSIC algorithm used in our research assumes that the noise covariance is some multiple of the identity matrix (*i.e.*, spatially isotropic). As mentioned earlier, the MUSIC algorithm may be extended to the case where the noise is not isotropic via use of a generalized eigendecomposition. Use of this extended MUSIC algorithm has the potential

to further lower the SNR threshold (the SNR above which the estimator performs satisfactorily) observed in our results.

A second way to improve localization performance involves modification of our cumulant-based MUSIC estimator. We noted earlier that an extended version of the cumulant matrix has been defined [Ref. 20]. Although an estimator based on this matrix would be more computationally intensive than the estimator defined here, it is expected to be less sensitive to estimation errors.

Refinement in the process of selecting suitable modes for MMP localization is a third means of improving the estimator. Although the simple approach described here was effective in generating an appropriate mode set for this environment, it may not produce results of the same quality in other environments. An approach relying more heavily on the propagation physics of the channel could greatly reduce the amount of "trial and error" involved in the process.

LIST OF REFERENCES

1. Bucker, H. P., "Use of calculated sound fields and matched-field detection to locate sound sources in shallow water," *J. Acoust. Soc. Am.*, **59**, 368–373, 1976.

2. Hinich, M. J., "Maximum likelihood signal processing for a vertical array,", *J. Acoust. Soc. Am.*, **54**, 499–503, 1973.

3. Baggeroer, A. B., Kuperman, W. A., and Schmidt, H., "Matched field processing: Source localization in correlated noise as an optimum parameter estimation problem," *J. Acoust. Soc. Am.* **83**, 571–587, 1988.

4. Wilson, G. R., Koch, R. A., and Vidmar, P. J., "Matched mode localization," *J. Acoust. Soc. Am.*, **84**, 310–320, 1988.

5. Yang, T. C., and Bogart, C. W., "Matched-mode processing for sparse three-dimensional arrays," *J. Acoust. Soc. Am.*, **95**, 3149–3166, 1995.

6. Fawcett, J. A., Yeremy, M. L., and Chapman, N. R., "Matched-field source localization in a range-dependent environment," *J. Acoust. Soc. Am.*, **99**, 272–282, 1996.

7. Zala, C., Barrodale, I., and Greening, M., "Investigation of algorithms for locating an acoustic source in shallow water", DREP Contractors Report Series 85-11, 1985.

8. Ozard, J. M., "Matched-field processing in shallow water for range, depth, and bearing determination: Results of experiment and simulation," *J. Acoust. Soc. Am.*, **86**, 744–753, 1989.

9. Naidu, P. S. and Ganesan, T., "Source localization in a partially known shallow water channel," *J. Acoust. Soc. Am.*, **98**, 2554–2559, 1995.

10. Daugherty, J. R., and Lynch, J. F., "Surface wave, internal wave, and source motion effects on matched field processing in a shallow water waveguide," *J. Acoust. Soc. Am.*, **87**, 2503–2526, 1990.

11. DelBalzo, D. R., Feuillade, C., and Rowe, M. M., "Effects of water-depth mismatch on matched-field localization in shallow water," *J. Acoust. Soc. Am.*, **83**, 2180–2185, 1988.

12. Feuillade, C., DelBalzo, D. R., and Rowe, M. M., "Environmental mismatch in shallow-water matched-field processing: Geoacoustic parameter variability," *J. Acoust. Soc. Am.*, **85**, 2354–2364, 1989.

13. Schmidt, H., Baggeroer, A. B., Kuperman, W. A., and Scheer, E. K., "Environmentally tolerant beamforming for high-resolution matched field processing: Deterministic mismatch,", *J. Acoust. Am.*, **88**, 1851–1862, 1990.

14. Shang, E. C., and Wang, Y. Y., "Environmental mismatching effects on source localization processing in mode space," *J. Acoust. Am.*, **89**, 2285–2290, 1991.

15. Tolstoy, A.., "Sensitivity of matched field processing to sound-speed profile mismatch for vertical arrays in a deep water Pacific environment," *J. Acoust. Soc. Am.*, **85**, 2394–2404, 1989.

16. Von Der Heydt, K., Kemp, J., Lynch, J. F., Miller, J. H., and Chiu, C.-S., "Barents Sea Shallow Water Tomography," *Sea Technol.*, 55–59, 1993.

17. Parsons, A. R., Bourke, R. H., Plueddemann, A. J., Chiu, C.-S., Lynch, J. F., Muench, R. D., Pawlowicz, R., and Miller, J. H., "The Barents Sea Polar Front in Summer," *J. Geophys. Res.* (in press).

18. Jin, G., Lynch, J. F., Chiu, C.-S., and Miller, J. H., "Acoustic normal mode coupling effects due to the Barents Sea Polar Front, with applications to acoustic tomography and matched field processing," *J. Acoust. Soc. Am.* (submitted).

19. Chiu, C. S., Miller, J. H., and Lynch, J. F., "Forward coupled-mode propagation modeling for coastal acoustic tomography," *J. Acoust. Soc. Am.* **99**, 793–802, 1996.

20. Porat, B. and Friedlander, B., "Direction Finding Algorithms Based on High-Order Statistics", *IEEE Trans. Signal Proc.*, **39**:9, 1991.

21. Cardoso, J.-F. and Molines, E., "Asymptotic performance analysis of direction-finding algorithms based on fourth-order cumulants," *IEEE Trans. Signal. Proc.*, **43**, 214–224, 1995.

22. Naidu. P. S. and Subramaniyan, R., "Direction of arrival estimation in the presence of distributed noise sources: Cumulant based approach," *J. Acoust. Soc. Am.*, **97**, 2997–3001, 1995.

23. Roy, R. H., *ESPRIT: Estimation of Signal Parameters via Rotational Invariance Techniques,* Ph.D. Dissertation, Stanford University, 1987.

24. Dugundji, J., "Envelopes and pre-envelopes of real waveforms," *IRE Trans. on Information Theory*, IT-4, 53–57, 1958.

25. Papoulis, A., *Probability, Random Variables, and Stochastic Processes,* 3rd ed., McGraw-Hill, 1991.

26. Knight, W. C., Pridham, R. G., and Kay, S. M., "Digital Signal Processing for Sonar", *Proc. IEEE,* **69**, 1451–1506, 1981.

27. Schuster, A., "On the Investigation of Hidden Periodicities with Application to a Supposed 26 Day Period of Meteorological Phenomena," *Terr. Magn.,* Vol. 3, pp. 13–41, Mar 1898.

28. Capon, J., "High resolution frequency wave number spectrum analysis," *Proc. IEEE*, **57**, 1408–1418, 1969.

29. Lacoss, R. T., "Data Adaptive Spectral Analysis Methods," *Geophysics*, v. 36, pp. 661–675, August 1971.

30. Schmidt, R. O., "Multiple emitter location and signal parameter estimation," *Proc. RADC Spectrum Estimation Workshop,* pp. 243–258, Griffiss AFB, N.Y., 1979.

31. Schmidt, R. O., *A Signal Subspace Approach to Multiple Emitter Location and Spectral Estimation,* Ph.D. Dissertation, Stanford University, 1981.

32. Schmidt, R. O., "Multiple emitter location and signal parameter estimation," *IEEE Trans. on Ant. and Prop.*, **34,** 276–290, 1986.

33. Golub, G. H., and Van Loan, C. F., *Matrix Computations*, Johns Hopkins University Press, 1989.

34. Shiryaev, A. N., "Some Problems in the Spectral Theory of Higher-Order Moments I", *Theory Probl. Appl.*, **5**, 265–284, 1960.

35. Brillinger, D. R., "An Introduction to Polyspectra", *Ann. Math. Statist.,* **36**, 1351-1374, 1965.

36. Brillinger, D. R., and Rosenblatt, "Computation and Interpretation of kth-Order Spectra," in *Spectral Analysis of Time Series*, B. Harris (ed.), pp. 189–232, Wiley, 1967.

37. Nikias, C. L., and Raghuveer, M. R., "Bispectrum estimation: a digital signal processing framework," *Proc. IEEE*, **75**, 869–891, 1987.

38. Mendel, J. M., "Tutorial on higher-order statistics (spectra) in signal processing and system theory: theoretical results and some applications," *Proc. IEEE*, **79**, 278–305, 1991.

39. Nikias, C. L. and Petropulu, A. P., *Higher-Order Spectral Analysis*, Prentice Hall, 1993.

40. Miller, K. S., *Complex Stochastic Processes*, Addison-Wesley, 1974.

41. Therrien, C. W., *Discrete Random Signals and Statistical Signal Processing*, Prentice Hall, 1992.

42. Clay, C. S. and Medwin, H., *Acoustical Oceanography*, p. 296, John Wiley & Sons, 1977.

43. Jensen, F. B., Kuperman, W. A., Porter, M. B., and Schmidt, H., *Computational Ocean Acoustics*, Springer-Verlag, New York, 1992.

44. Chiu, C.-S., Miller, J. H., Denner, W. W., and Lynch, J. F., "A three-dimensional, broadband, coupled normal-mode sound propagation modeling approach," in *Full Field Inversion Methods in Ocean and Seismic Acoustics*, Kluwer Acad., Dordrecht, 57–62, 1995.

45. Chiu, C. S., and Ehret, L. L., "Computations of sound propagation in a three-dimensionally varying ocean—a coupled mode approach," in *Computational Acoustics: Ocean-Acoustic Models and Supercomputing* (Lee, Cakmak and Vichnevetsky, eds.), Elsevire (North-Holland), 187–202, 1990.

46. Tolstoy, A., *Matched Field Processing for Underwater Acoustics*, World Scientific, Singapore, 1993.

47. Maranda, B. H., and Fawcett, J. A., "The Localization Accuracy of a Horizontal Array Observing a Narrowband Target with Partial Coherence," *IEEE J. Oc. Eng.*, **18**, 466–473, 1993.

48. Kinsler, L. E., Frey, A. R., Coppens, A. B., and Sanders, J. V., *Fundamentals of Acoustics*, John Wiley & Sons, 3rd ed., 1982.

49. Shang, E. C., "Passive harmonic source ranging in waveguides by using mode filter," J. Acoust. Soc. Am. **78** (1), 1985.

50. Shang, E. C., "Source depth estimation in waveguides," J. Acoust. Soc. Am. **77** (4), 1985.

51. Yang, T. C., "A method of range and depth estimation by modal decomposition," *J. Acoust. Soc. Am.* **82** (5), 1987.

52. Yang, T. C., "Effectiveness of mode filtering: A comparison of matched-field and matched-mode processing," *J. Acoust. Soc. Am.* **87**, 2072-2084, 1990.

53. Muggleworth, C. E., "Shallow water reverberation and measurement," Master's Thesis, Naval Postgraduate School, 1994.

54. Kay, S. M., *Modern Spectral Estimation: Theory and Application*, Prentice Hall, 1988.

INITIAL DISTRIBUTION LIST